Hybrid Machine Learning for Integrating Pedological Knowledge into Digital Soil Mapping to Advance Next-Generation Earth System Models

Rodrigo de Q. Miranda[1,2,*], Rodolfo L. B. Nóbrega[3,4,*], Estevão L. R. da Silva[2,5], Jadson F. da Silva[2], José C. de Araújo Filho[5], Magna S. B. de Moura[6], Alexandre H. C. Barros[5], Alzira G. S. S. Souza[7], Anne Verhoef[8], Wanhong Yang[1], Hui Shao[1], Raghavan Srinivasan[9,10], Feras Ziadat[11], Suzana M. G. L. Montenegro[12], Maria do S. B. Araújo[13], and Josiclêda D. Galvíncio[2]

[1]University of Guelph, Department of Geography, Guelph, Ontario, N1G 2W1, Canada

[2]PRODEMA, Universidade Federal de Pernambuco, Recife, Brazil

[3]University of Bristol, School of Geographical Sciences, University Road, Bristol BS8 1SS, UK

[4]Imperial College London, Georgina Mace Centre for the Living Planet, Department of Life Sciences, Silwood Park Campus, Buckhurst Road, Ascot, SL5 7PY, UK

[5]Brazilian Agricultural Research Corporation – Embrapa Soils, Recife, Pernambuco, Brazil

[6]Brazilian Agricultural Research Corporation – Embrapa Semi-arid Region, Petrolina, Pernambuco, Brazil

[7]Federal Institute of Education, Science and Technology of Bahia, 45680-000, Uruçuca, Bahia, Brazil

[8]The University of Reading, Department of Geography and Environmental Science, Reading, UK

[9]Spatial Sciences Laboratory, Texas A&M University, College Station, USA

[10]Blackland Research and Extension Center, Agrilife Research, Temple, USA

[11]Food and Agriculture Organization of the United Nations (FAO), 00153 Rome, Italy

[12]Dept. de Engenharia Civil, Universidade Federal de Pernambuco, Recife, Pernambuco, Brazil

[13]Departamento de Ciências Geográficas, Universidade Federal de Pernambuco, Recife, Brazil

Corresponding author: Rodolfo L. B Nóbrega (r.nobrega@bristol.ac.uk)

*These authors contributed equally to this work.

Key Points:

- We developed a hybrid machine learning framework for mapping multiple soil properties with low prediction redundancies and high accuracy.
- This framework enables the interpretation of the morphology and environmental modulators of the soil spatial distribution.
- Our methodology is transferable to other regions, facilitating the mapping of soil properties to be used in Earth System models.

Abstract

Land surface and Earth System models require reliable soil maps to represent the influence of spatial variability of soil properties on ecosystem fluxes and storages. However, mapping soils using conventional in situ survey protocols is time-consuming and costly. We addressed the outdated spatial information on soil physico-chemical properties for a tropical region with a ~700-km longitudinal gradient of contrasting topography, climate, and vegetation (~98,000 km^2; NE Brazil), by developing a novel hybrid machine learning framework and applying it to this region. This framework reduces prediction redundancies due to high multicollinearity by implementing a recursive feature selector algorithm for input selection; its core is composed of the Soil-Landscape Estimation and Evaluation Program (SLEEP) and a calibrated Gradient Boosting Model (GBM) capable of modeling the spatial distribution of soil properties at multiple and dynamic soil depths. The use of SLEEP and GBM allowed us to explain the spatial distribution of various soil properties and their environmental modulators. The model training and testing approach used six topographical, ten meteorological and two vegetation properties, and data from 223 soil profiles across the study area. Our models demonstrated a consistent performance with spatial extrapolations exhibiting r^2 values of 0.79–0.98, and -1.39–1.14% percent bias. The properties related to topography and climate were dominating when estimating the number of soil layers, soil texture, and the sum of bases. Our framework features high flexibility and it is transferable to other tropical regions, while reducing capital investments and increasing accuracy when compared to traditional mapping protocols.

Plain Language Summary

Computer models that predict environmental processes require accurate soil information, which is obtained from soil maps. However, traditional techniques for creating these maps are time-consuming and expensive. Digital Soil Mapping (DSM) is an alternative approach that utilizes a fast-mapping technique to estimate soil properties over large areas with greater efficiency and accuracy. Here, we produced digital soil maps for a highly diverse tropical region in Brazil. We developed a machine learning framework that combined the Soil-Landscape Estimation and Evaluation Program (SLEEP) and a Gradient Boosting Model (GBM), to predict the distribution of soil properties based on a combination of topographical, meteorological, vegetation, and soil sample data from 223 locations. Our results showed that the model had consistent spatial performance, achieving high correlation values and low errors. Topographic and climatic conditions were the most important factors in estimating the number of soil layers, soil texture, and soil fertility.

1 Introduction

Soils are a key component in many landscape models that focus on providing solutions to global environmental issues such as food and water scarcity, unsustainable energy production, and biodiversity losses (Bouma & McBratney, 2013). For a more comprehensive understanding of the role of soils in these global challenges, as well as its interactions with other environmental factors, it is necessary to robustly map the spatial distribution of soil properties. Soil mapping is complex and has been one of the most time demanding and expensive tasks in soil science (Li & Heap, 2014; Mendonça-Santos & dos Santos, 2006). Most of the existing maps were produced using the conventional soil survey protocol (Hartemink et al., 2012), which remains the most adopted approach to record the highly variable soil properties in landscapes. However, this surveying approach has been criticized for being heuristically dependent on the practical knowledge of pedologists and for deriving interpretations using sometimes insufficient or incomplete datasets (Scull et al., 2003).

Digital Soil Mapping (DSM) is an integrated complementary alternative that has been increasingly gaining adoption as a tool to map soil properties. DSM reduces both survey time and costs (Kempen et al., 2012; McBratney et al., 2003), and it improves the accessibility to soil data with more frequent updates (Lagacherie & McBratney, 2006); it consists of establishing statistical relationships between field information obtained from soil point sampling and environmental data related to soil forming processes, e.g., relief, climate, parent material, and vegetation parameters, to produce models capable of extrapolating data with high resolution (Scull et al., 2003). Numerous studies in Europe (Ballabio et al., 2016; Poggio & Gimona, 2017; Tóth et al., 2017), Africa (Akpa et al., 2016; Ramifehiarivo et al., 2017), North and South America (Guevara et al., 2018; Hartemink et al., 2012; Padarian et al., 2017), and Oceania (Gray et al., 2016; Teng et al., 2018) used DSM to reduce soil mapping costs over large areas. More specifically, some of them used 3D radar products to acquire high spatial resolution soil information either through data extrapolation using regressors (Adhikari et al., 2014) or disaggregation with machine learning (ML) techniques (Ellili-Bargaoui et al., 2020). Some of these studies contributed to existing regional datasets (Teng et al., 2018) or global datasets such as the GlobalSoilMap project (Ballabio et al., 2016; Rahmati et al., 2018). Others analyzed and discovered new relationships between soil properties and soil-forming processes (Ramifehiarivo et al., 2017). DSM has also been used to find potential hotspots for carbon sequestration and to support sustainable land management strategies, while providing high quality datasets that are widely applicable (Akpa et al., 2016; Gray et al., 2016; Guevara et al., 2018). These data can be coupled with mathematical functions to estimate soils properties for a range of socioeconomical purposes such as water and agricultural management, design of crop rotation scenarios, and urban planning (Nketia et al., 2022; Padarian et al., 2017).

The methodological core of DSM includes mathematical models capable of performing spatial extrapolations of soil properties at multiple spatial scales (Barros et al., 2013; Laurent et al., 2017; Saxton & Rawls, 2006; Tomasella et al., 2000; Q. Wang et al., 2018; Zeraatpisheh et al., 2019). These models can predict the distribution of a given soil property horizontally, e.g., over the topsoil of a landscape, or vertically, i.e., along soil profiles. In soil science, spatial extrapolations are usually made by (i) applying a conceptual model to the survey area to simulate the distribution of soil patches (Scull et al., 2003), (ii) using geostatistical interpolations (Li & Heap, 2014), (iii) delimiting geographical subdivisions where environmental processes follow a relatively homogeneous pattern, such as the facets described by (Ziadat et al., 2015), or (iv) by applying pedotransfer functions (PTFs) to properties of each soil location. PTFs are predictive mathematical equations that aim to use basic soil information to derive other soil properties that are often costly to measure, such as the water retention curve, or related parameters, e.g., field capacity and wilting point (Barros & de Jong van Lier, 2014). When combining both above-mentioned types of predictive tools to perform 3D extrapolations, high uncertainties are expected, especially for the vertical extrapolations because information is required across the soil profile that is rarely available (Yost & Hartemink, 2020).

Land surface and Earth System models require reliable data on soil hydraulic and thermal properties, which are often obtained via PTFs (Dai, Xin, et al., 2019; Turek et al., 2022). (Paschalis et al., 2022) have shown that both soil textural properties and PTFs are a source of high uncertainty when modeling carbon and water fluxes. Thus, there is an ever-growing need for soil data, especially in the tropics where data on soil properties is scarce (Minasny & Hartemink, 2011;

Scharlemann et al., 2014) and where soils are the most diverse in the world (Orgiazzi et al., 2016). In Brazil, many polynomial PTFs have been calibrated at both national (Tomasella et al., 2000) and sub-national scales (Barros et al., 2013; L. B. Oliveira et al., 2002). However, for many soil properties or geographic regions, certain PTFs might not provide sufficiently accurate parameter estimates due to their excessive number of polynomial terms that lead to overfitting (Hawkins, 2004). For example, mathematical regressions calibrated for temperate climate zones and applied to the tropics often do not return realistic soil parameters, e.g., (Tomasella & Hodnett, 1998). These applications may lead to improper soil use and management recommendations. To avoid misapplications that produce inconsistent soil maps, it is important to develop robust geostatistical relationships between predictive models and regional characteristics (Barros & de Jong van Lier, 2014).

Compared to popular linear regression models, ML techniques have been increasingly applied as an approach to circumvent issues due to conventional DSM methods and the complexity in modeling the soil with ever-increasing amounts of information stored in databases on soil parameters and covariates (Wadoux et al., 2020). These techniques include a set of models capable of detecting non-linear patterns, such as generalized linear models (Begueria et al., 2013), random forest (Esfandiarpour-Boroujeni et al., 2020; Pahlavan-Rad et al., 2020; Poppiel et al., 2021), cubist (Taghizadeh-Mehrjardi et al., 2016), and support vector machine (Esfandiarpour-Boroujeni et al., 2020). These models have been successfully applied to generate a wide variety of data types, which is compelling because soil properties often do not follow a normal distribution, but an exponential, Poisson, Bernoulli or uniform distribution instead (Hitziger & Ließ, 2014). If trained properly, ML techniques allow for accurate predictions, whereas other approaches with underlying assumption on distributions may not be applicable or even fail to produce any values (Taghizadeh-Mehrjardi et al., 2016), e.g., a regression may require the calculation of the square root or logarithm of negatives values. In fact, (Behrens et al., 2018) suggest that ML techniques might even eliminate the need for further steps to correct biases during the mapping process because they commonly only produce residuals that do not exhibit any spatial dependence.

The use of ML in DSM can provide updated soil products for improving modeling performance in land surface models, e.g., CABLE (Y. P. Wang et al., 2011), JULES (Best et al., 2011; Clark et al., 2011) and ORCHIDEE (Krinner et al., 2005), and some widely applied hydrological models, e.g., Soil and Water Assessment Tool (SWAT; (Arnold et al., 1998), and Soil and Water Integrated Model (SWIM; Krysanova et al. (2005). Bossa et al. (2012) evaluated the impact of different soil mapping concepts in hydrological models and demonstrated that it strongly influences modeling outputs. In this context, the mapping approach and the soil database scale are important and directly affect many modeling steps (Bossa et al., 2012). Thus, environmental modeling and other soil data applications need adequate spatial characterization of soil properties (Montzka et al., 2017; Ziadat et al., 2015). However, most of the ML studies used for soil mapping do not predict a soil property class for multiple depths, and, when they do, it is common to follow specifications, such as the GlobalSoilMap (Arrouays et al., 2014), which disregard consistency with respect to existing pedological knowledge and, consequently, interpretation of the results is limited (Wadoux et al., 2020). The correct representation of the structure of soils produce substantial improvements in environmental models, which is being systematically neglected in Earth System models (Fatichi et al., 2020).

The possibility of using high-resolution environmental covariates offers new opportunities for adding local information into the modeling of soil properties (Gupta et al., 2021). In hydrology, for example, SWAT uses the algorithm of the Soil-Landscape Estimation and Evaluation Program (SLEEP; (Ziadat et al., 2015) to generate a suite of standard environmental covariates that can be easily assimilated in the hydrological modeling process. However, the use of covariates alone often use simple multiple regressions that fail to capture both gradual and abrupt changes in soil variation (Wadoux et al., 2020). The use of ML techniques, i.e., random forest (RF) or gradient boosting models (GBMs), has improved the prediction accuracy of soil organic matter when compared to geostatistical methods, and it was even further improved when both methods were combined as a hybrid approach (Tziachris et al., 2019). More recently, Gupta et al. (2021), with a focus on land surface modelling applications, used a hybrid ML approach that improved saturated hydraulic conductivity predictions over PTF-based methods. They generated a final dataset with a spatial resolution of 1 km, and they argued that both resolution and quality of the dataset can be improved with more data availability and initiatives to estimate soil and environmental covariates at higher spatial resolutions. In their approach, they combined soil variables with environmental covariates on climate, terrain, surface reflectance, vegetation, and soil by using a RF algorithm and data from 821 sites distributed around the world; in total, they used 6,814 measurements with only ~12% from the tropics. Indeed, soil maps for the tropics often shows a coarse spatial soil property aggregation, which generalizes soil variability into average values. This occurs because the common statistical techniques applied to perform extrapolations are heavily dependent on how dense the collection of soil profiles is; and this is generally sparse due to financial and temporal limitations.

In this study, we addressed the growing need for soil models that produce improved information about the spatial variability of soil physical and chemical properties in the tropics, by developing a novel hybrid machine learning (HML) framework for DSM and applying to a tropical region with a ~700-km longitudinal gradient of contrasting topography, climate, and vegetation. By focusing on this region, we are not only addressing a long-standing lack in observations from the tropics in global soil databases and datasets, but also testing and proving a trained framework that is highly transferable to other tropical areas that lack a good representation in land surface and Earth System models. The hybrid framework's core is composed of the (SLEEP) and a calibrated GBM capable of modeling the spatial distribution of soil properties at multiple soil depths. Our goal was to develop and validate a hybrid framework that integrates GBM with a soil landscape attribute model that allowed for: (a) assimilating legacy soil data; (2) predicting and comparison of spatial distributions of physical and chemical properties soil properties at a high spatial resolution (30 m); (3) the interpretation of pedological characteristics (e.g. number of soil layers and their respective depths) and major environmental modulators of the soil spatial distribution in this region, and; (4) producing off-the-shelf soil datasets for direct input in environmental models.

2 Materials and Methods

2.1 Methodology Overview

We developed and applied a HML framework integrating SLEEP and a calibrated GBM. HML can be understood as a seamlessly combination of algorithms from different areas of knowledge to complement each other for higher predictive power than a standalone ML algorithm, e.g., Artificial Neural Network and Vector Support Machine. By integrating SLEEP and GBM, we created a promising framework capable of predicting soil data over large areas. Our methodology for applying the framework comprises a three-step process that starts with the collection and pre-processing of six topographical, ten meteorological, and two vegetation properties acquired from different data sources ranging from remotely sensed datasets to meteorological stations. These are the independent variables to be correlated with *in situ* soil physical and chemical properties (described in section 2.6) to make subsequent horizontal and vertical predictions of these basic soil properties.

We used the Soil-Landscape Estimation and Evaluation Program (SLEEP; (Ziadat et al., 2015) to create a non-distributed grid formed by facets, which, in this study, are treated as the smallest area that reflect a single homogenous unit where soil formation factors might produce homogeneous types of soils. To define these facets, SLEEP create first creates preliminary versions of these facets by delineating watersheds. Each watershed is divided into multiple catchments, and then the facets are defined by the division of the catchments into two parts, i.e., each side of their main drainage stream (Ziadat et al., 2015). The size of the catchments is determined by a user-defined threshold assigned during stream definition. The smaller this threshold, the denser is the stream network, resulting in a greater number of delineated catchments and facets. Once the facets are created, SLEEP aggregates them based on their slope similarity in a process called facet classification, which ultimately creates contiguous patches. The patches allow SLEEP to reduce the number of facets by grouping them in a single mapping unit. These are especially useful to reduce the processing time when working with large areas, and to avoid the 'salt-and-pepper' noise in the mapping process. Then, we simulated the basic soil properties in each patch at multiple depths by calibrating one model for each soil basic property using ML instead of traditional SLEEP simple multiple regressions because they can capture a wider range of data distributions. The calibration mechanism is composed of a recursive feature selector and a randomized searcher, which were configured to perform a 2-fold cross-validation. At the end of this step, all patches are turned into virtual soil profiles, namely simulated soil patches with their own depth-dependent simulated physical and chemical properties. The uncertainty was calculated for each property to characterize the error consistency for each simulated value. Finally, in the third step, the entire dataset composed of virtual profiles was complemented with further simulated soil parameters obtained with a range of PTFs, and an analysis of the relationship between our estimates and the land-use of the study area. The entire modeling algorithm developed and applied in this study is freely available at https://github.com/razeayres/sleepy in Python versions 2.7.15 and 3.6.9 (Miranda, Nóbrega, & Galvíncio, 2022).

2.2 Study Area

The study area is in the Northeast Brazil; it covers an area of approx. 98,000 km^2, and closely follows the domain of the state of Pernambuco (Fig. 1). This region exhibits a longitudinal gradient of contrasting topography, climate and vegetation. The elevation ranges from approx. 0 to over 1,150 m a.s.l. in a variable gradient from East to West. This region is influenced by three meteorological phenomena, namely Frontal Systems (FS), Upper Tropospheric Cyclonic Vortices (UTCV), and the Inter Tropical Convergence Zone (ITC) (Salgueiro et al., 2016). There are three predominant climate types (Köppen's classification) in the study are: hot semi-arid (steppe) climate (BSh; 61.4% of the area), tropical with dry summer (As; 32.7%) and tropical monsoon (Am; 4.9%); the remaining 1% is composed of areas with a tropical climate with dry winter (Aw; 0.1%), humid subtropical with dry winter and hot (Cwa; 0.3%) and temperate summer (Cwb; 0.3%), and with dry and hot summer (Csa; 0.3%) (Alvares et al., 2013). Precipitation has a high spatial variability (Souza et al., 2021) with the annual mean precipitation rates reaching approx. 2,000 mm in the East, and decreasing westwards to less than 400 mm. As for the vegetation, near the coast, the predominant land-uses are Atlantic rain forest and rainfed croplands, which are composed of a mosaic of sugarcane plantations and fruticulture (C. M. Souza Jr et al., 2020). With the climate becoming drier, the vegetation changes to a seasonally dry tropical forest, i.e., the Brazilian Caatinga. Pastures become a common land-use activity, and the soil gets shallower and rocky (C. M. Souza Jr et al., 2020). In the middle transition, some high-altitude areas create microclimatic conditions that favor rainfed crops of corn and beans, and mixed natural vegetation formations. According to the Brazilian system of soil classification (and FAO system of soil classification), the dominant soils are, respectively, *Argissolos* (i.e., Acrisols and Lixisols) (25% of the area), *Neossolos* (i.e., Leptosols, Arenosols, Regosols, or Fluvisols) (32%) and *Planossolos* (i.e., Planosols and Solonetz) (16%), *Latossolos* (i.e., Ferralsols) (9%) and *Luvisolos* (i.e., Luvisols) (9%) (Araújo Filho et al., 2014). The geology maps for the state of Pernambuco show predominantly (90%) pre-Cambrian rocks belonging to the São Francisco Craton and the Borborema Province, and the remaining area is mainly composed by Paleomesozoic sedimentary basins and Mesocenezoic coastal basins (Torres & Pfaltzgraff, 2014).

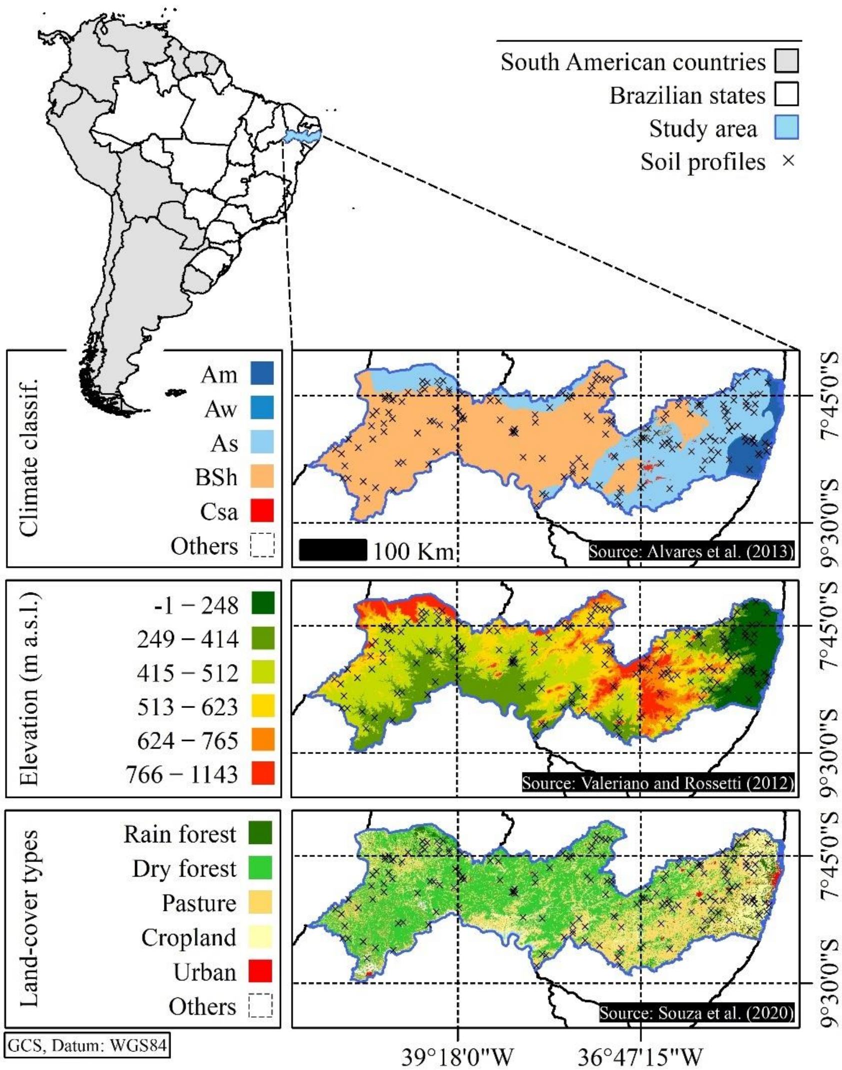

Figure 1. Spatial distribution of the surveyed soil profiles across a longitudinal gradient of environmental conditions over the study area.

2.3 Input data collection

We selected the input parameters based on their widely known role on soil formation. **Elevation data:** we collected data from the TOPODATA database (http://www.dsr.inpe.br/topodata), which is a bias-corrected version of the data produced by the NASA SRTM (Shuttle radar topography mission) for the Brazilian territory made by the National Institute of Spatial Research (INPE). The data were spatially refined from 3 (approx. 90 m) to 1 arc-second (approx. 30 m) using adjusted kriging models, and it was tested on 40 Brazilian areas with distinct geological settings (de Morisson Valeriano & de Fátima Rossetti, 2012). **Soil data:** we digitalized georeferenced data regarding morphological (number and depth of soil horizons), physical (particle size distribution) and chemical (Ca^{2+}, Mg^{2+}, K^{+}, Na^{+} and C) properties of the soil were acquired from the Agroecological Zoning of the state of Pernambuco (ZAPE) project of the Brazilian Agricultural Research Corporation (EMBRAPA). The ZAPE project focused on the production and organization of a georeferenced database with information on soils, climate, and vegetation that can be used in multiple applications, including sustainable land-use management and agricultural purposes (Silva et al., 2001). The legacy soil database comprises 223 soil profiles distributed over the study area (Fig. 1). **Auxiliary meteorological data:** we obtained data for air temperature (°C), air relative humidity (%), solar radiation (MJ m^{-2} day^{-1}), wind speed (m s^{-1}), and precipitation (mm) from the 1961–2016 period through two open-access databases: daily precipitation data from the Water and Climate Agency of Pernambuco (APAC; http://www.apac.pe.gov.br/meteorologia/monitoramento-pluvio.php), and the other meteorological parameters from the National Water Agency of Brazil (ANA; https://www.snirh.gov.br/hidroweb/). **Auxiliary remote sensed data:** we obtained data regarding NDVI (Normalized Difference Vegetation Index) (MOD13A3; composition: monthly, spatial resolution: 1 km) (Didan, 2015), and LST (Land Surface Temperature) (MOD11A2; composition: 8-days, spatial resolution: 1 km) (Wan et al., 2015) from https://earthdata.nasa.gov/ (Greenbelt, 2019).

Table 1. Summary of variables and parameters with their corresponding descriptions and units.

Variable	Type	Description	Unit
AAT	T	Prefix used to denote accumulated variables	-
ASPECT	T	Downslope direction at each cell	°
CTI	T	Compound Topographic Index	-
CURV	T	Curvature of the surface at each cell	-
DEM	T	Digital elevation model	m
PCTSLP	T	Slope of the surface at each cell	%
LST	V	Land surface temperature	K
NDVI	V	Normalized difference vegetation index	-
DEWPT	C	Mean air relative humidity	fraction (0–1)
PCPMM	C	Mean total monthly precipitation	mm
PCPSKW	C	Skew coefficient for daily precipitation in month	mm
PCPSTD	C	Standard deviation for daily precipitation in month	mm
SOLARAV	C	Mean daily solar radiation for month	MJ m^{-2} day^{-1}
TMPMN	C	Mean daily minimum air temperature	°C
TMPMX	C	Mean daily maximum air temperature	°C
TMPSTDMN	C	Standard deviation for daily minimum air temperature	°C
TMPSTDMX	C	Standard deviation for daily maximum air temperature	°C
WNDAV	C	Mean daily wind speed in month	m s^{-1}
CS	B	Coarse sand content	%
FS	B	Fine sand content	%
L_MAX	B	Number of soil layers	-

SB	B	Sum of bases (Ca^{2+}, Mg^{2+}, K^{+} and Na^{+})	$cmol_c\ kg^{-1}$
SN1	B	Non-sand content	fraction
SOL_BD	B	Moist bulk soil density	$g\ cm^{-3}$
SOL_CBN	B	Organic carbon content	%
SOL_CLAY	B	Clay content	%
SOL_ROCK	B	Rock fragments content	%
SOL_SAND	B	Sand content	%
SOL_SILT	B	Silt content	%
SOL_Z	B	Depth from soil surface to bottom of the soil layer	mm
R_v	P	Volume fraction of gravel	$cm^3\ cm^{-3}$
R_w	P	Weight fraction of gravel	$g\ g^{-1}$
θ_{1500}	P	Water content at -1500 kPa	$m^3\ m^{-3}$
θ_{33}	P	Water content at -33 kPa	$m^3\ m^{-3}$
θ_S	P	Saturated water content	$m^3\ m^{-3}$
θ_r	P	Residual water content	$m^3\ m^{-3}$
ρ_N	P	Normal density	$g\ cm^{-3}$
ρ_R	P	Gravel density	$g\ cm^{-3}$
OM	P	Organic matter	%
SOL_AWC	P	Available water capacity of the soil layer	$mm\ mm^{-1}$
SOL_K	P	Saturated hydraulic conductivity	$mm\ hr^{-1}$
USLE_K	P	USLE equation soil erodibility (K) factor	-
Ψ	P	Matric potential	kPa
α, n and m	P	Shape-fitting parameters of (van Genuchten, 1980)	-

In column 2: T = topography, V = vegetation, C = climate, B = basic property, and P = pedotransfer function parameter.

2.4 Soil survey data description

Our soil dataset consists of the total number of soil horizons (L_MAX), but for the modelling purposes in this study we will be referencing it as the number of soil layers as we did not validate model efficacy on distinguishing horizons with further field experiments. The database also has each soil layer depth from the land surface (SOL_Z; mm), soil clay content (< 0.002 mm; SOL_CLAY; %), silt (> 0.002 and < 0.05 mm; SOL_SILT; %), sand (> 0.05 and < 2 mm; SOL_SAND; %), rock (> 2 mm; SOL_ROCK; %), organic carbon (SOL_CBN; %) and sum of bases (sum of Ca^{2+}, Mg^{2+}, K^{+} and Na^{+}; SB; $cmol_c\ kg^{-1}$). In this study, we define the rock parameter as the sum of the fractions of gravel (> 2 mm and < 2 cm), cobbles (> 2 cm and < 20 cm), boulders (> 20 cm and < 100 cm) and rocks (> 100 cm). The sand fraction was divided into coarse (> 0.2 and < 2 mm; CS) and fine (> 0.05 and < 0.2 mm; FS) (Table 1). All particle classification followed the Brazilian technical standards described in ABNT (1995), and physical and chemical analysis were performed as described in (Embrapa, 1997).

Soil profiles exhibit an average total depth of 1,228 ± 613 mm, ranging from 120 to 2,550 mm. The number of soil layers varies from one to seven and correlates well ($r^2 = 0.89$, p-value < 0.01) with the profile depth (SOL_Z). Rocks exhibit 4.4 ± 11% of total content, and when they are not considered by the soil texture is composed by sand (55 ± 19%), clay (27 ± 14%), and silt (18 ± 9%) (Fig. 2). The low silt content is typical of tropical environments, and it is a common property in the Northeast region of Brazil (Barros et al., 2013; Ottoni et al., 2018), where most sandy soils originate from the quaternary era, and the clayey ones from tertiary and early cretaceous eras (Araujo Filho et al., 2000). These textural patterns determine differences in hydraulic properties between soils in tropical and temperate regions (Ottoni et al., 2018). For this reason, PTFs developed for temperate climates often provide inaccurate or unrealistic estimates when applied to the tropics (Barros et al., 2013; Tomasella et al., 2000). Organic carbon contents are higher (0.54

± 0.49%) than the values found by Barros et al. (2013) for the Northeast region of Brazil (0.35%), and lower than the ones for the entire Brazilian territory (0.91 ± 0.78%) (Tomasella et al., 2000).

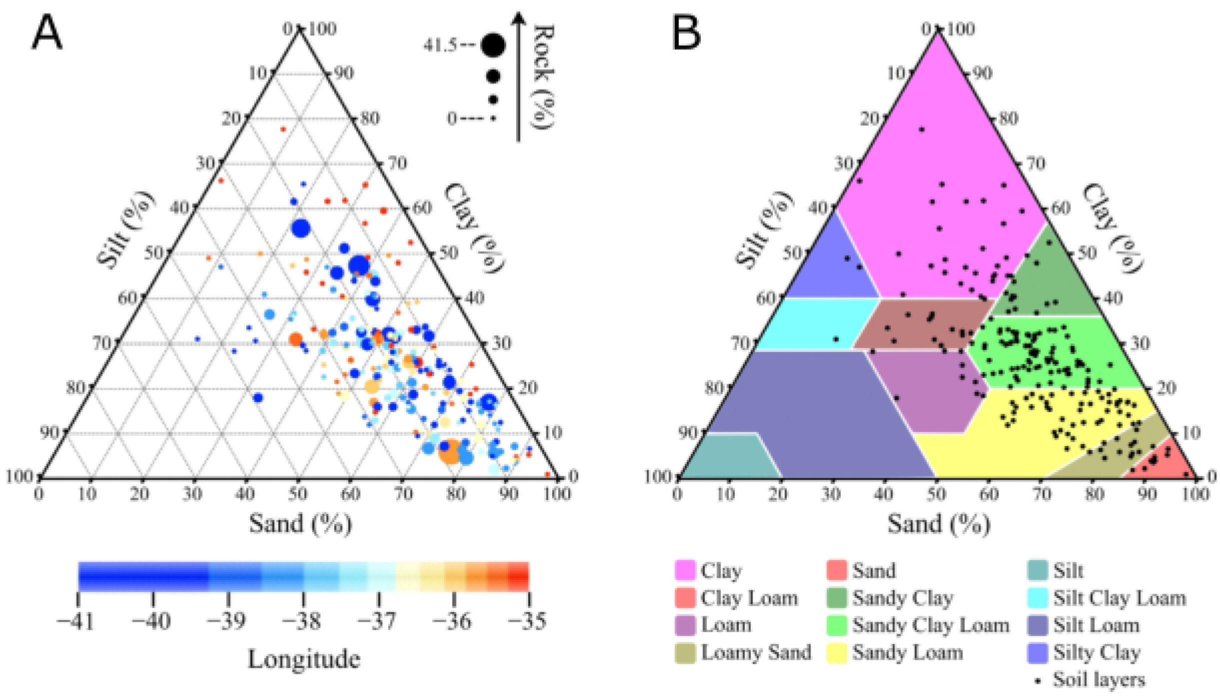

Figure 2. Soil textural distribution for sand, silt and clay upscaled to 100% after removing the fraction of rocks, which is exhibited separately in (a).

2.5 Input preprocessing workflow

As a first step, the data for each soil layer from each soil profile (total of 925 soil layers) were converted into a shapefile. We estimated the organic matter (OM) by multiplying SOL_CBN by 2, as recommended by (Pribyl, 2010). For all meteorological parameters (Table 1), we calculated means and standard deviations for all months in the data series (multiple months) and considered the maximum and minimum air temperatures as distinct parameters; then the monthly statistics were summed (in case of precipitation) or averaged resulting in 12 historical values. In addition to these statistics, we calculated the skewness of rainfall data distribution following the same logic of temporal aggregation (PCPSKW) using the following equation:

$$\mathrm{PCPSKW} = \frac{d_W \times \sum_{d=1}^{d_W} (P_d - \bar{P})^3}{(N-1)\times(N-2)\times\sigma^3} \quad (1)$$

Here d_W is the count of wet days in a month, N is the number of daily data records for a month, P_d is the precipitation on a given day in mm, $\bar{P}$ is the monthly average precipitation, and σ is its standard deviation. For all calculations we only considered years without gaps in the data series for each meteorological station individually, and from these data we derived ten parameters that were used in a spatial interpolation. This interpolation was conducted using the inverse distance weighting (IDW) method at a fixed cell resolution of 0.05°. This method was chosen due to its representativeness in variable terrain area and wide adoption for climate data interpolation, e.g., Tan et al. (2021). Additionally, we performed a leave-one out cross-validation and extracted details on the accuracy of these interpolations (Table 2). As for the remotely sensed data, mosaics and reprojections were created using the MODIS Reprojection Tool, and scaling and processing of the historical annual images were conducted using the GDAL library (https://gdal.org/). The scaling factors for each product were acquired from the relevant user guides available at https://lpdaac.usgs.gov/.

Table 2. Leave-one-out cross-validation leave-one out of all interpolated meteorological input parameters. The description of the variables can be found in Table 1.

Parameters	Power	Samples	r^2	RMSE	PBIAS
PCPMM (mm)	1.64	6140	0.94	21.34	-0.10
PCPSTD (mm)	1.65	6140	0.83	2.62	-0.17
PCPSKW (mm)	1	6140	0.87	1.33	0.03
TMPMX (°C)	1.63	254	0.94	1.51	0.19
TMPMN (°C)	1.77	254	0.95	1.43	0.88
TMPSTDMX (°C)	2.32	254	0.97	0.24	-0.51
TMPSTDMN (°C)	1	254	0.95	0.30	-0.18
SOLARAV (MJ m^{-2} day^{-1})	1.46	254	0.94	1.00	-0.24
DEWPT (0–1)	1.66	254	0.92	0.04	0.38
WNDAV (m s^{-1})	1.82	254	0.89	1.25	-0.0001

2.6 Input preprocessing workflow

The core of the HML framework combines the SLEEP and a calibrated GBM. Soil data were modeled using the SLEEP model by creating facets, for which basic soil properties, i.e., L_MAX, SOL_Z, SOL_CLAY, SOL_SILT, SOL_SAND, CS, FS, SOL_ROCK, SOL_CBN, and OM, were calculated. The SLEEP model requires three different types of inputs: (i) a digital elevation model (DEM), (ii) a shapefile containing the data observed for each soil profile, and (iii) the auxiliary data including meteorological and vegetation data in raster format (Fig. 3) (Ziadat et al., 2015). In this algorithm, we extract the drainage network following (Tarboton et al., 1991) by using the size of the catchments to represent 0.001% of the total study area, i.e., on average 1,803 pixels per catchment, which was obtained based on a visual evaluation of different thresholds with a focus on providing high resolution data and satisfactory model processing time. We aggregated the facets based on their slope similarity using the clustering technique Iso Cluster (Richards, 2013) to create patches. Finally, we modified the way the basic properties are modeled, changing it from simple multiple linear regressors from the original SLEEP algorithm to GBMs (Fig. 4). GBM is an ensemble learner that consists of a set of decision trees composed by weak-prediction models (WPM) often prone to overfitting, and, when combined, produces highly accurate outputs. Each of these trees is a rule-based system, where their terminal nodes can either be a WPM, i.e., leaf, or an if-then-else rule over a given input variable, i.e., regular node. The whole trees are created using an iterative sequence of improvements of WPMs, i.e., boosting, while optimizing themselves by reducing a loss function, i.e., gradient (Natekin & Knoll, 2013).

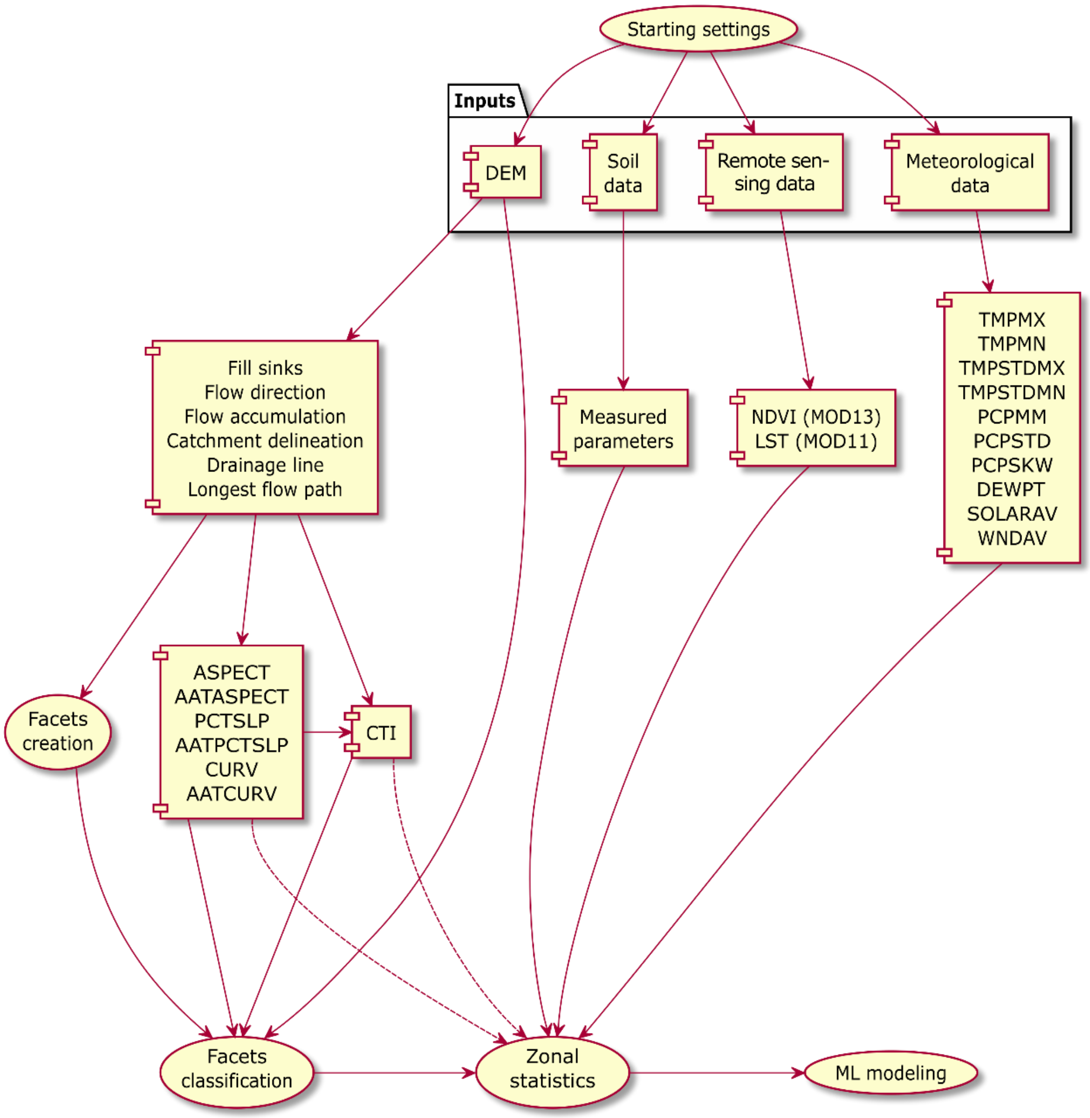

Figure 3. Processing scheme of the integration of the SLEEP algorithm and the Gradient Boosting Models. The description of the parameters can be found in Table 1.

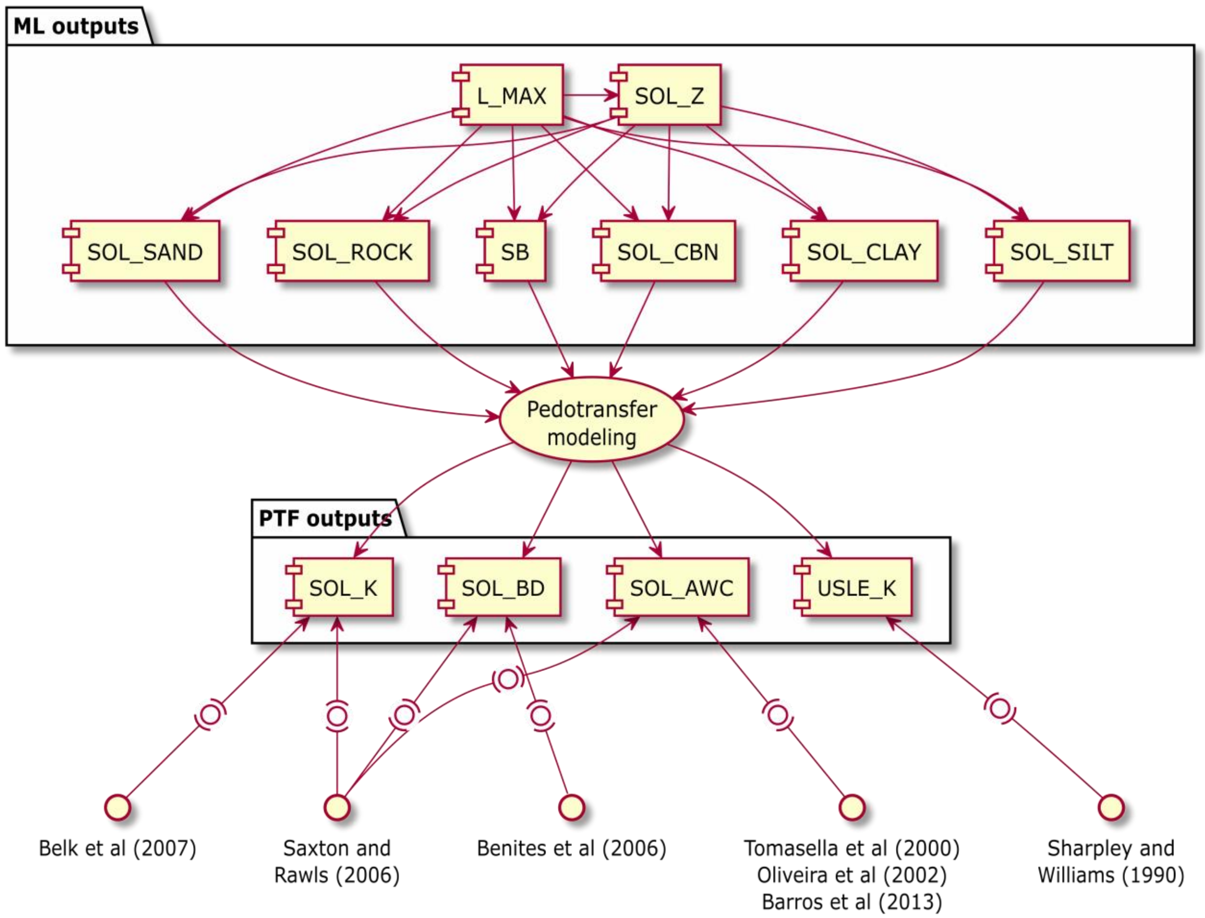

Figure 4. Processing workflow of all model outputs. The top half of this figure explains the machine learning processing of the basic soil characteristics, whereas the bottom half summarizes the PTF-derived products. The description of the parameters can be found in Table 1.

For the GBM processing, two datasets were produced: (i) one composed of only the information from the patches that overlay the observed data for each profile (dataset for fitting), and (ii) consisting of all available input information for every patch in the study area (dataset for prediction). The dataset for fitting was split using the Holdout method at 20%, e.g., (Whitney, 1971), creating two sub-datasets, where 80% of the records were used for model calibration (training dataset), and the remaining for further model verification (verification dataset) (Fig. 5). The sampling technique used in this process is a variation of the k-fold cross-validation (Wong, 2015), which returns stratified folds containing approximately the same percentage of samples of each target class. When dependent variables were continuous, without classes, a quantile-based discretization function (QCUT) was applied to discretize these variables into equal-sized groups based on sample quantiles, allowing for sampling the entire data distribution. The GBMs had four basic parameters derived from the DEM (Table 1) as input features, namely the downslope direction (ASPECT), the Compound Topographic Index (CTI), the curvature of the surface (CURV) and the slope of the surface (PCTSLP). The CTI is represented by a steady state wetness index as a function of the slope and the upstream contributing area (Moore et al., 1993), and 12 auxiliary data series from remote sensing products and meteorological stations. As targets, they had eight basic soil properties. All inputs and targets are described in Table 1. GBM was used as a multiclass classifier to simulate the number of soil layers, L_MAX; and as regressors for the other targets. SOL_ROCK was estimated as a residual of all textural parameters. Coarse sand (CS) and fine sand (FS) were resampled to total 100%.

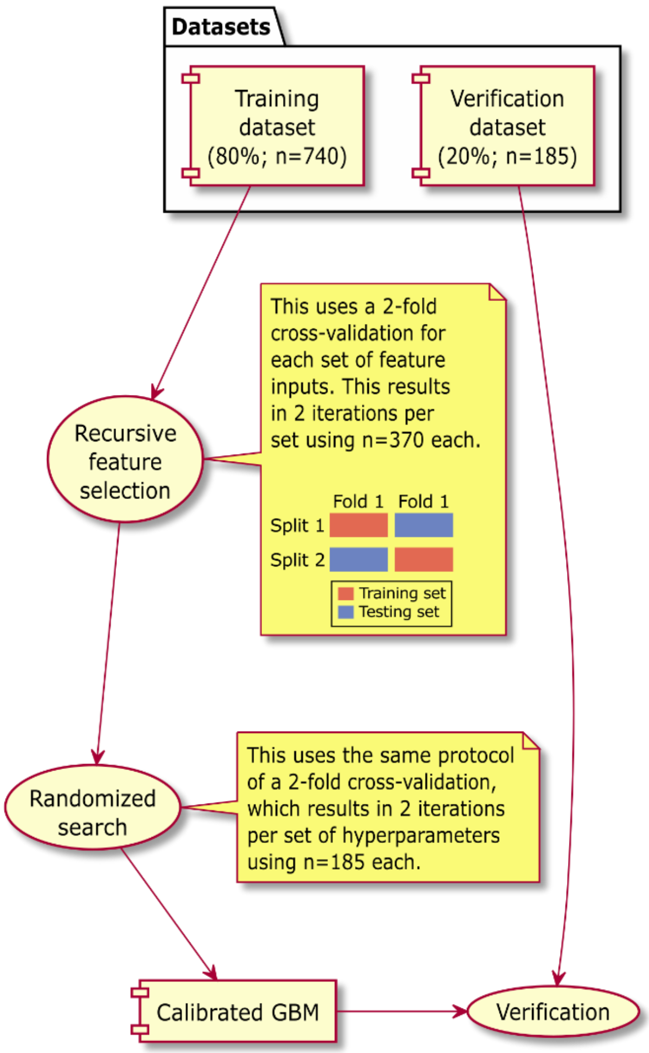

Figure 5. Machine learning processing design for modeling the basic soil properties.

GBMs are often parameterized with only a few control inputs called hyperparameters. They hold the potential to define the final structure of the model and its predictive strength. These hyperparameters must be calibrated; for that purpose, we submitted all our GBMs to a recursive feature selector (RFS; (Guyon et al., 2002) configured to perform cross-validation using the k-fold cross-validation at 2-folds, and then a randomized 2-fold calibration to search for the best combination of hyperparameters. The RFS here is an input feature selection algorithm that fits a model and eliminates the weakest ranked inputs recursively, considering each iteration a smaller set of features until the best combination found. The performance indices used in all calibrations were the accuracy (Eq. 2) for the classifiers, i.e., L_MAX, and the coefficient of determination (r^2) (Eq. 3) for the regressors. Further in the analysis, for model verification, the most efficient models were compared to the testing dataset, and the same performance indices plus the Root Mean Square Error (RMSE) (Eq. 4) and Percent Bias (PBIAS) (Eq. 5) were applied. This final verification allowed us to evaluate the potential of the best models to perform extrapolations.

$$\textbf{Accuracy} = \frac{(\boldsymbol{TP}+\boldsymbol{TN})}{(\boldsymbol{TP}+\boldsymbol{FP}+\boldsymbol{FN}+\boldsymbol{TN})} \qquad (2)$$

$$\mathrm{r}^2 = \frac{\sum(obs-\overline{obs})\times(sim-\overline{sim})}{\sqrt{\sum(obs-\overline{obs})^2}\times\sqrt{\sum(sim-\overline{sim})^2}} \qquad (3)$$

$$\mathrm{RMSE} = \sqrt{\frac{\sum(obs-sim)^2}{n}} \qquad (4)$$

$$\mathrm{PBIAS} = \frac{\sum(obs-sim)}{\sum(obs)} \times 100 \qquad (5)$$

TP, FP, FN and TN are the number of True Positives, False Positives, False Negatives and True Negatives, respectively, in a contingency table; obs is the observed value of a given soil layer, and sim is the simulated one, and $\overline{obs}$ and $\overline{sim}$ are average values. Accuracy is a metric of evaluation for classification problems that works well only if the data distribution is not skewed. We then applied the Synthetic Minority Oversampling Technique (SMOTE) to our dataset to solve all possible imbalances by producing a new dataset that has a uniform distribution. This technique forces a balanced learning and an overall better class detection. It introduces biases towards the minority classes by adding more samples to the model learning process from these classes. Details of this technique can be found in (Chawla et al., 2002). To calibrate the hyperparameters, we created a set of possible values for each parameter. For n_estimators (NE; number of trees in the forest), it was composed of 100 values varying from 10 to 5,000; for max_depth (MD; maximum number of levels in each decision tree) it was 100 values in the 1–100 interval; and min_samples_leaf (MSL; minimum number of data for a node to persist) and min_samples_split (MSS; minimum number of data placed in a node required to perform a split) were both set to 49 values, varying between 2–50. These four hyperparameters control the potential for overfitting. If n_estimators is excessively high, then the GBM exhibits a robust performance during calibration but has a poor predictive strength during extrapolations. Also, n_estimators must be determined for each individual application, and directly affects the learning rate and processing time. Small values for max_depth are desirable to avoid models learning very localized relations that cannot be accurately extrapolated. The same applies to min_samples_leaf to solve imbalances in samples distribution successfully. The value of min_samples_split has a similar effect as max_depth on the model performance, but here higher values are best to avoid relations highly specific to samples selected for a given tree. These effects are well described in (F. Dormann et al., 2007), (Elith et al., 2008) and (Hitziger & Ließ, 2014). The entire hyperparameter tuning was set to run 4,000 simulations. The calibrated models were applied to predict the basic properties for each patch, creating 64,415 virtual soil profiles. The entire predicted dataset was converted to raster format, and each raster is a different soil attribute. All outputs are available from Miranda, Nóbrega, da Silva, et al. (2022).

2.7 Sensitivity and uncertainty analysis

The model sensitivity to input data was calculated as the importance, i.e., a weighted factor of each selected property for the most accurate GBMs. The importance (w) ranges from 0 to 1, where 1 reflects the highest weight a given input can receive in a model, and 0 the lowest. The sum of all weights is 1 for each model. More specifically, w values reflect indirectly how much the performance metric changes every time a given input is used to split a node in the whole model (Natekin & Knoll, 2013).

For the uncertainty analysis of the modeled variables, the selected inputs for each model and patch used in the predictions were classified into two categories (e), i.e., whether they extrapolated the calibration range of values (1) or not (0), as summarized in the following equation:

$$u_f = \sum_{i=0}(e_i \times w_i), \quad (6)$$

where u_f is the uncertainty of each model; patch, e_i, is the binary category that reflects the extrapolation and w_i is its importance in the model (weight) of a given selected input i. As u_f gets close to 1, extrapolation is greater and so is its associated uncertainty. The contrary happens when it approaches 0, which means that all inputs used for a given prediction were in the range of values used for calibration.

2.8 Application and comparison of pedotransfer functions

All data from the virtual soil profiles were submitted to a series of pre-established PTFs to estimate four soil properties: SOL_BD (moist bulk density; g cm^{-3}), SOL_AWC (available water capacity; mm mm^{-1}), SOL_K (saturated hydraulic conductivity; mm hr^{-1}), and USLE_K (factor K from the USLE equation; unitless) with the primary purpose of producing these derived datasets and making them available. SOL_K and USLE_K were modeled using the equations described in Saxton & Rawls (2006) and Belk et al. (2007), and Sharpley et al. (1993) (Eqs described in Table S1 in the Supporting Information). The calculation of SOL_AWC created a factorial design in our analysis. It was acquired with the equations from Saxton & Rawls (2006), Tomasella et al. (2000), Oliveira et al. (2002) and Barros et al. (2013) (described in Eq groups S7 and S8 in the Table S2 in the Supporting Information). Saxton & Rawls (2006) produced PTFs using a soil dataset from an exhaustive soil sampling across the entire United States. Tomasella et al. (2000) used a similar database for Brazil, while Barros et al. (2013) used data for the Northeast region of Brazil only. Finally, Oliveira et al. (2002) created PTFs with data that originated strictly from the state of Pernambuco. All SOL_AWC models require SOL_BD as an input. Thus, SOL_BD from Saxton & Rawls (2006) was coupled with their own SOL_AWC model, while SOL_BD from Benites et al. (2006) was used in the models ofTomasella et al. (2000), Oliveira et al. (2002) and Barros et al. (2013). This resulted in 32 different complete sets of PTFs that can be used to estimate the five soil properties.

We compared our SOL_K results using Saxton & Rawls (2006) to the dataset generated by Gupta et al. (2021), who generated high-resolution, i.e., 1 km, global SOL_K values using a hybrid ML framework. We chose Saxton & Rawls (2006) because it is a widely used PTF. We avoided bias of comparing Gupta et al. (2021)'s results to PTFs that were adjusted to our area of study, such as from Barros et al. (2013) and Oliveira et al. (2002). Nevertheless, we made available all results of all PTFs and their combinations, e.g. using the SOL_K model from Saxton and Rawls (2006) using the field capacity model from Barros et al. (2013), at https://zenodo.org/deposit/5918544 (Miranda, Nóbrega, da Silva, et al., 2022). To allow the SOL_K comparison, we have cropped the dataset from Gupta et al. (2021) to our spatial extent, and resampled our dataset to Gupta et al. (2021)'s spatial resolution. We also compared the clay fraction obtained in this study and the one used by Gupta et al. (2021) available from Hengl (2018) because this is an important component of many SOL_K models, including Saxton and Rawls (2006) (Table S2 in the Supporting Information). We calculated mean SOL_K and clay fraction as a weighted mean for each grid cell for their SOL_K and respective soil depth since our SOL_K values are representative for the entire soil layer. For the SOL_K dataset from (Gupta et al., 2021) and clay fraction from Hengl (2018) we calculated its mean using the trapezoidal rule suggested by Hengl et al. (2017) because the SOL_K values were predicted at specific soil depths and not intervals.

2.9 Land-use data collection and spatial statistics

To exemplify one of the many potential applications using our results, we performed zonal statistics on the modeled soil textural attributes to analyze their distribution over multiple land-use types. For that, we acquired annual land-use maps from 1985 to 2019 via the API of the MAPBIOMAS project in the Google Earth Engine (GEE; https://earthengine.google.com/). The MAPBIOMAS is an integrated initiative from Brazilian researchers to reconstruct land use and cover changes in Brazilian Biomes, using Landsat Archive and cloud computing capabilities (C. M. Souza Jr et al., 2020). They were able to map forest and non-forest natural formation, farming, non-vegetated areas, and water bodies for the entire country at high spatial resolution (30 m). The overall accuracy of the final MAPBIOMAS product is 89% (C. M. Souza Jr et al., 2020). Detailed tutorials on how to acquire all data can be found at https://mapbiomas.org/.

To analyze differences in soil texture among distinct land-use classes, we first submitted all 35 maps to an intercept geoprocessing tool in the package QGIS 3.10.3 (downloadable at https://qgis.org/), producing a raster where its pixels reflect the areas where no changes in land use occurred during the 1985–2019 period, i.e., zonal raster. Then, we used this zonal raster to acquire spatial statistics of the soil texture attributes per land use class.

3 Results and discussion

3.1 Model approximation

The spatial modeling produced 64,415 patches with an average area of 1.35 ± 4.54 km^2, and an average density of 0.75 patches per km^2. Each one of these were considered as a virtual soil profile for which GBM outputs were calculated. When working with DSM, having a high level of model predictive ability is essential because of the inductive nature of the soil mapping science, where patterns in observations are found and declared to be a general model (Overmars et al., 2007). However, preventing overfitting is important due to the nature of successive boosting inherent in GBMs, which allows decision trees to be added until the model is completely overfitted (F. Dormann et al., 2007). To avoid this from happening, the structure of the trees must be tuned by adjusting the models hyperparameters. This structure is usually calibrated by applying a calibration algorithm with a range of possible values for each hyperparameter ($b_{i,min}$–$b_{i,max}$). In this study, the models demonstrated a consistent ability to perform such extrapolations as the performance of the models during the verification were similar to those found by the calibration algorithm (Table 3). The r^2 and PBIAS values varied from 0.79 to 0.98, and from -1.39 to 1.14, respectively. Among all models for textural properties, the lowest r^2 value was found for the modeled SOL_SILT (0.79). We believe that the large number of predictors, each with similar importance, for the SOL_SILT model (Table 4) may have caused prediction redundancies, and probably degraded the model strength by increasing its variance, even though we applied a RFS algorithm for feature selection. All model outputs and respective metadata are freely available from (Miranda, Nóbrega, da Silva, et al., 2022).

Table 3. Calibrated values for the hyperparameters n_estimators (NE), max_depth (MD), min_samples_split (MSS) and min_samples_leaf (MSL) of the Gradient Boosting Models (GBM) of basic soil properties, and their calibration performance. The description of the variables can be found in Table 1.

Output	Calibrated hyperparameters				Calibration	Verification		
	NE	MD	MSS	MSL	Accuracy[(a)] or $r^{2(b)}$	Accuracy[(a)] or $r^{2(b)}$	RMSE	PBIAS
L_MAX	1325	23	41	70	0.91[(a)]	0.96[(a)]	-	-
SOL_Z (mm)	4445	3	36	7	0.92[(b)]	0.98[(b)]	73.19	0.02
SOL_SAND (%)	2521	87	73	6	0.77[(b)]	0.91[(b)]	6.27	1.14
SOL_CLAY (%)	1518	38	85	12	0.78[(b)]	0.93[(b)]	4.48	0.29
SOL_SILT (%)	1624	85	15	3	0.76[(b)]	0.79[(b)]	4.77	-1.36
SOL_CBN (%)	1265	27	17	43	0.78[(b)]	0.91[(b)]	0.14	-3.39
SB ($cmol_c\ kg^{-1}$)	1026	46	23	2	0.82[(b)]	0.95[(b)]	1.79	2.97
CS (%)	2893	38	40	63	0.92[(b)]	0.98[(b)]	2.46	1.04
FS (%)	2282	3	7	13	0.89[(b)]	0.97[(b)]	2.03	-0.03

When comparing descriptive statistics between the simulated and observed reference datasets, differences are expected since the observed dataset was not created using a systematic sampling, thus there are spaces with singular environmental properties that were not captured in our observed dataset. The highest differences were found for SOL_ROCK (44.5%), SB (53.1%), CS (103.3%) and FS (31.9%). Even without a systematic sampling approach, these values should not be excessively high since the observed dataset still covers the entire study area and a high diversity of environments (Table 4). We attribute these high differences in SOL_ROCK to the calculation of the parameter as a residual of all textural parameters, which was not directly modeled. As for CS and FS, they were directly modeled but unavoidably resampled to a total of 100%. We did not use the same technique for the texture parameters, and choose to sacrifice SOL_ROCK prediction accuracy, because its spatial variance produces a high number of zeros (38.5% of the total values) in comparing to all other parameters (< 0.01%), leaving not enough variance to perform any modeling accurately. Although SB exhibited no zeros in the dataset, it produced a similar effect on regressors as SOL_ROCK did because 21.98% of its values ranged between 0.1 and 3.84 $cmol_c\ kg^{-1}$, presenting an exponential data distribution. Finally, 51.49% of the 135,934 virtual profiles exhibited some uncertainty. Most of the uncertainty was under 15% and its highest value was of 51.49% (Fig. 6).

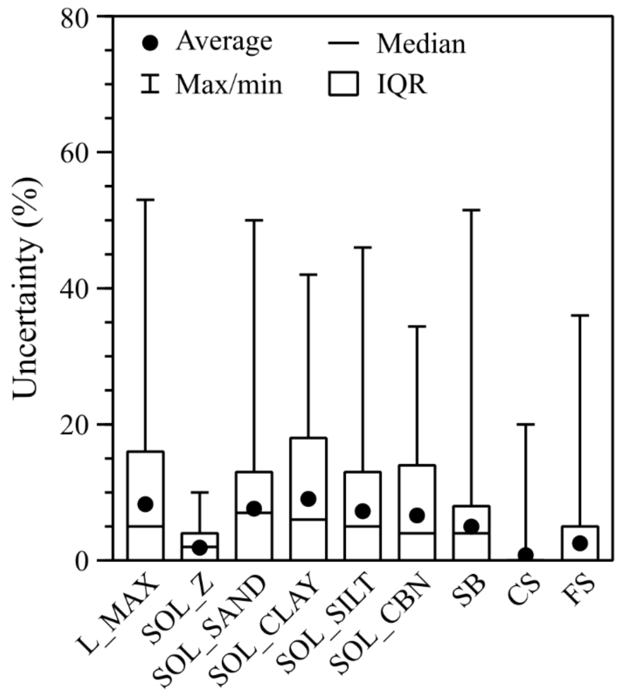

Figure 6. Uncertainty analysis of the Gradient Boosting Models (GBM) of the basic soil parameters for the estimates whose inputs extrapolated the calibration range of values. The description of the variables can be found in Table 1.

Table 4. Descriptive statistics of the Gradient Boosting Models of basic soil properties, with the reference observed values between parentheses. The description of the variables can be found in Table 1.

Basic property	Mean±SD		Minimum		Maximum	
L_MAX	4±1	(4±1)	1		(1)	
SOL_Z (mm)	700.88±475.26	(737.36±559.63)	1	(50)	8	(8)
SOL_SAND (%)	46.77±13.08	(51.52±21.27)	0	(0)	3051.4	(2550)
SOL_CLAY (%)	28.87±11.7	(27.3±17.51)	0	(0)	97.09	(98)
SOL_SILT (%)	17.99±6.4	(16.78±10.67)	0	(0)	83.6	(83.6)
SOL_ROCK (%)	6.37±7.89	(4.41±10.63)	0	(0)	56.92	(59)
SOL_CBN (%)	0.58±0.36	(0.54±0.49)	0.0002	(0)	100	(100)
SB ($cmol_c$ kg^{-1})	10.67±7.76	(6.97±8.39)	0.01	(0.14)	3.38	(3.38)
CS (%)	67.96±9.66	(29.51±18.46)	0	(0)	46.11	(49.74)
FS (%)	32.03±9.65	(24.28±13.09)	0	(0.4)	100	(88)

Reference observed values within parentheses.

The models developed in this study used a dataset of *in situ* observations from a range of different climates, vegetation covers and topographical characteristics. This dataset produced the variance required by the GBM; and was a key element in applying the framework successfully. These results show that our framework is easily transferable to other tropical regions within a similar range of environmental modulators. This framework can also be applied to regions regions with different characteristics since multiple variations of a single parameter can be used as long as it does not violate the assumption of multi-collinearity. When applying our methodology to regions with different characteristics, we recommend performing a simple dataset splitting test to evaluate whether the models are being fed with an appropriate (*i*) number of samples, and (*ii*) quality dataset, i.e., whether it has a sufficient variance. Normally, the model performance is not heavily affected by an increase in the number of samples in a dataset, as it prevents corruption of its variance. However, if the sample size is small — this is a region-specific characteristic and can be only evaluated by performing tests — the overall variance will be easily impacted by individual samples.

3.2 Environmental modulators

Results showed that the soil properties were relatively sensitive to climate, topographic, and vegetation properties (Fig. 7). Understanding how these environmental factors affect the physical and chemical soil properties can support the management of their changes in response to future climate conditions or deforestation (Badía et al., 2016). In our study area, the properties related to topographic and climatic conditions were dominating when estimating all attributes, whereas the properties regarding vegetation were especially strong for the soil property estimates related to sand, i.e., SOL_SAND, CS and FS. Topography is always present as input variables in our models (Table 5), and it is indeed an important factor in soil formation in Northeast Brazil (Oliveira et al., 2018). The topographic conditions can be divided into the slope, which may affect the quantity of soil deposition or erosion; the aspect, which drives the water flux direction over the soils, and relative exposure of the soils to sunlight; and the curvature, which changes flow velocity, controlling the erosion and deposition processes (Barbieri et al., 2009; Patton et al., 2018).

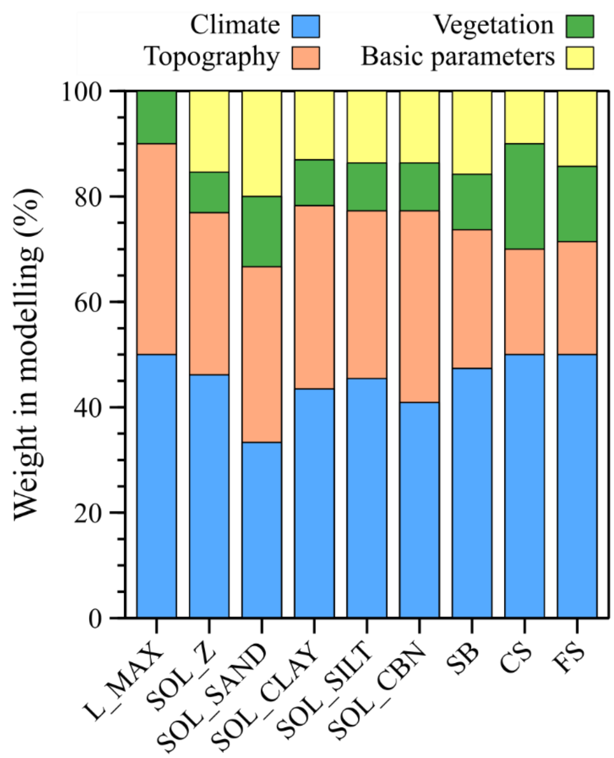

Figure 7. Proportional weights (w, as in Eq. (6)) of the different types of inputs for modeling each basic soil parameter. The description of the variables can be found in Table 1.

Table 5. List of input parameters used for calibrating the Gradient Boosting Models of basic soil properties. The weights (w) calculated for each input in the models are between parentheses. The description of the variables and parameters can be found in Table 1.

Output	Inputs
L_MAX	NDVI (0.18), DEM (0.13), ASPECT (0.07), PCPMM (0.07), WNDAV (0.07), AAT_ASPECT (0.05), CUR (0.05), TMPSTDMX (0.05), TMPMX (0.04), ATT_CUR (0.03), CTI (0.03), SPR (0.03), PCPSTD (0.03), TMPMN (0.03), TMPSTDMN (0.03), ATT_SPR_F (0.02), LST (0.02), PCPSKW (0.02), DEWPT (0.02), SOLARAV (0.02).
SOL_Z	LAYER (0.83), AAT_ASPECT (0.02), CUR (0.02), NDVI (0.02), DEM (0.02), TMPMN (0.02), L_MAX (0.02), CTI (0.01), PCPSKW (0.01), PCPMM (0.01), SOLARAV (0.01), WNDAV (0.01), TMPSTDMN (0.01).
SOL_SAND	NDVI (0.09), WNDAV (0.09), CTI (0.08), LST (0.08), SOL_Z (0.08), ASPECT (0.07), CUR (0.07), TMPMN (0.07), PCPSKW (0.06), DEM (0.06), LAYER (0.06), ATT_CUR (0.05), TMPMX (0.05), TMPSTDMN (0.05), L_MAX (0.05).
SOL_CLAY	AAT_ASPECT (0.08), PCPMM (0.08), LST (0.07), ASPECT (0.06), CUR (0.06), WNDAV (0.06), DEM (0.05), CTI (0.04), NDVI (0.04), PCPSTD (0.04), ATT_CUR (0.03), DEWPT (0.02), SOLARAV (0.02), TMPSTDMX (0.02), TMPMN (0.02), TMPSTDMN (0.02), ATT_SPR_F (0.01), SPR (0.01), PCPSKW (0.01), TMPMX (0.01).
SOL_SILT	TMPMN (0.11), SOL_Z (0.1), DEM (0.09), ASPECT (0.07), PCPMM (0.07), CTI (0.05), CUR (0.05), DEWPT (0.05), L_MAX (0.05), AAT_ASPECT (0.04), ATT_SPR_F (0.04), NDVI (0.04), SOLARAV (0.03), TMPSTDMX (0.03), TMPSTDMN (0.03), LAYER (0.03), SPR (0.02), LST (0.02), WNDAV (0.02), TMPMX (0.02), PCPSKW (0.01), PCPSTD (0.01).
SOL_CBN	LAYER (0.24), SOL_Z (0.2), ATT_CUR (0.07), NDVI (0.06), CUR (0.04), WNDAV (0.04), AAT_ASPECT (0.03), CTI (0.03), SPR (0.03), PCPSKW (0.03), PCPSTD (0.03), PCP_MM (0.03), DEM (0.03), ASPECT (0.02), ATT_SPR_F (0.02), LST (0.02), SOLARAV (0.02), TMPMN (0.02), TMPSTDMN (0.02), L_MAX (0.02), DEWPT (0.01), TMPSTDMX (0.01).
SB	DEWPT (0.19), WNDAV (0.14), PCPSTD (0.08), DEM (0.07), SOL_Z (0.07), TMPMN (0.06), LST (0.05), TMPSTDMX (0.05), ASPECT (0.04), CUR (0.04), PCPMM (0.04), L_MAX (0.04), AAT_ASPECT (0.03), TMPSTDMN (0.03), NDVI (0.02), LAYER (0.02), ATT_CUR (0.01), SOLARAV (0.01), TMPMX (0.01).
CS	SOL_SAND (0.65), TMPSTDMX (0.06), DEM (0.05), TMPMX (0.05), SPR (0.04), LST (0.04), NDVI (0.04), SOLARAV (0.03), WNDAV (0.03), PCPSTD (0.02).
FS	SOL_SAND (0.4), SOLARAV (0.09), NDVI (0.07), ATT_CUR (0.05), SPR (0.05), DEM (0.05), TMPMX (0.05), TMPSTDMX (0.05), LST (0.04), PCPMM (0.04), DEWPT (0.03), TMPSTDMN (0.03), SOL_Z (0.03), WNDAV (0.02).

Our model for SB was mainly influenced by relative air humidity (19%) and wind speed (14%). These variables are known for controlling the intensity of biochemical reactions, and wind erosion (Ravi et al., 2004), and are capable of moving nutrients and thus affect its local content. Although precipitation may be an important climate factor for soil formation in other regions, e.g., (Dixon et al., 2016), its characteristics, i.e., PCPSTD and PCPMM, counted only for 12% of our model for SB, and the low r^2 (0.34) between DEWPT and PCPMM suggests that relative air humidity was not used due to a potential correlation to rainfall. At high relative humidity, soil chemicals weather relatively quickly, and this is an extremely favorable condition to biochemical reactions, which may increase the yields of organic matter, and limit the partitioning of organic chemicals into the soil (Eppes et al., 2020; Truu et al., 2017). In addition, air humidity affects erosion, as soil particles may become more aggregated. This is explained by the effect of hygroscopic forces and their dependence on soil matric potential, especially in dry soils (Davarzani et al., 2014; Ravi et al., 2004). For the wind speed, it may change the contents of topsoil nutrients (T. M. Zobeck et al., 1989), especially in arid and semi-arid regions, as seen in the west region of our study area, where soils are dry and covered by a sparse vegetation (Ravi et al., 2004).

The L_MAX model had NDVI (18%) and terrain elevation (13%) as its main inputs. Although the elevation is a topographic variable, it often modulates climate conditions as it is related to physical features that may create ‘climate islands’ (Badía et al., 2016), either by the processes of rain shadows or via changes on atmospheric lapse rates (Nettesheim et al., 2015). Thus, it is well related to meteorological conditions (Badía et al., 2016), which impact the speed at which parent materials weather, and hence the rate of soil development. As for NDVI, it reflects indirectly the vertical variability in the soil, as soils formed under forests tend to be more weathered. It happens because forests grow in higher rainfall areas (Bonan, 2008).

Other model inputs include CTI and the basic parameters themselves, which, in our case, are L_MAX, SOL_Z and SOL_SAND. CTI is especially important when predicting various soil properties, as it encapsulates the terrain structure (Gessler et al., 1995; Moore et al., 1993). The SOL_SAND and SOL_SILT estimates were strongly modulated by the SOL_Z. Sand formation is well reported to occur on top layers that are more vulnerable to erosion (Valentin & Bresson, 1992). Silt content variations are mainly driven by the temperature profile in the soil that affects soil aeration though changes in producing CO_2, and soil structure by modulating interactions among the clay particles, yielding less clay and more silt in deeper layers. The SOL_SAND also showed a moderate relationship with the vegetation inputs. The vegetation cover is a potential indicator of weathered soils, or reduced sand contents, as soils formed under dense forests are usually in high-rainfall areas (Souza et al., 2016), as seen the eastern region of our study area.

3.3 Hydraulic parameters

The moist bulk density estimates SOL_BD_{SR} (Saxton and Rawls, 2006) and SOL_BD_{OL} (Benites et al., 2006) were similar, with mean differences of only 0.11 g cm^{-3} (Table 6). These models produced an acceptable range of values since other studies in Brazil have found a maximum variation between 0.13 and 2.25 g cm^{-3}, e.g., Benites et al. (2007) and Boschi et al. (2018). In general, PTFs tend to be over-adjusted, to varying degrees, to the dataset used in their calibration step (De Vos et al., 2005). For the SOL_AWC, i.e., the SOL_AWC_{OL} from Oliveira et al. (2002), which was calibrated strictly using data from our study area, was the only equation that did not saturate when simulations were performed. As we evaluate and map soils for a common region to Oliveira et al. (2002), these results highlight the overfitting trend that usually exists in PTFs.

Table 6. Descriptive statistics of all calculated pedotransfer functions (PTF) data using basic soil properties derived from Gradient Boosting Models (GBM). Table 1 contains the description of acronyms.

PTF outputs	Mean (SD)		Minimum	Maximum	Invalid values (%)
SOL_BD_{SR} (g cm^{-3})	1.54	(0.09)	1.01	2.23	0
SOL_BD_{OL} (g cm^{-3})	1.45	(0.07)	1.12	1.76	0
SOL_AWC_{SR} (mm mm^{-1})	0.11	(0.01)	0.01	0.18	0
SOL_AWC_{BR} (mm mm^{-1})	0.05	(0.03)	0.001	0.17	0.75
SOL_AWC_{TM} (mm mm^{-1})	0.03	(0.01)	0.001	0.13	5.01
SOL_AWC_{OL} (mm mm^{-1})	0.07	(0.01)	0.01	0.16	0

SOL_K_{SR} (mm hr^{-1})	11.17 (14.24)	0.003	932.54	0
$SOL\_K_{SR/BR}$ (mm hr^{-1})	1,101.28 (350.5)	10.41	1,900.21	0
$SOL\_K_{SR/TM}$ (mm hr^{-1})	26.72 (26.58)	0.001	219.47	12.07
SOL_K_{BK} (mm hr^{-1})	63.85 (333.9)	8.85	12112	0
USLE_K (unitless)	0.22 (0.03)	0.01	0.41	0

Two of the four estimates of SOL_K were variations of Saxton and Rawls (2006) (Tables S1 and S2 in the Supporting Information). The difference between them is in the calculation of the inputs θ_S, θ_{33} and θ_{1500}, which differs from the approaches originally proposed by Saxton and Rawls (2006), SOL_K_{SR}, by Barros et al. (2013), $SOL\_K_{SR/BR}$, and by Tomasella et al. (2000), $SOL\_K_{SR/TM}$. Maximum values ranged from 219.47 ($SOL\_K_{SR/TM}$) to 12,112 mm h^{-1} ($SOL\_K_{SR/BR}$). SOL_K_{BK} is the simplest approach; it only uses SOL_Z as input, and therefore it does not show differences for soils with different textures that have the same depths. Invalid values were found only for $SOL\_K_{SR/TM}$ due to inaccurate extrapolations, i.e., out of the a-priori parameter range, of θ_r and n, which produced negative values and exponents in the model. For USLE_K, the applied model expects values varying from 0.1 to 0.5 (Sharpley et al., 1993), but we reached values below this threshold. This happened because our simulated dataset contains soils with high coarse-sand contents.

The SOL_K dataset from Gupta et al. (2021) predominantly exhibited higher values when compared to our SOL_K estimates using the PTF from Saxton and Rawls (2006) (Fig. 8A). Although the discrepancy is up to five orders of magnitude in some areas (indicated by dashed rectangles in Fig. 8A), the highest density of differences is approximately five-fold (Fig. 8B). For the region with the most humid climate (Am climate in Fig. 1, rectangle 4 in Fig. 8A), we also found a higher clay content (up to 50%) in our dataset (Fig.8C), which we identify as one of the reasons for the SOL_K differences between the datasets for this specific area, despite a lack of overall high correlation between clay fraction differences and differences in SOL_K for the entire study region (Fig. 8D). The arid areas with highest differences in SOL_K (Fig. 8A, rectangles 1–3) exhibit one of the shallowest soils (Fig. 8E). Although we cannot draw a direct relationship between the SOL_K differences and soil depth, it is important to note that deeper soils in this region hold higher clay fractions (Fig. 8F). (Gupta et al., 2021)'s dataset follows a standardized soil layer protocol with a total depth of 200 cm for all grid cells, whereas our results were produced following a methodology that provide pedological meaning with a more realistic number of soil layers and respective depths. The impact of these differences goes beyond the disparities in saturated hydraulic values, which themselves carry high uncertainties (Zhang & Schaap, 2019). Estimates of hydraulic properties — even when satisfactory — can be highly misleading if the soil layers and depth are being assumed spatially homogeneous (Dai, Shangguan, et al., 2019). A better representation of the soil profile characteristics in models, such as soil depth (Brunke et al., 2016), will produce more realistic soil maps, as we have shown here, and thereby more reliable performance of Earth System models (Dy & Fung, 2016; Kearney & Maino, 2018).

We acknowledge that only 12% of the measurements used to train the ML algorithm that generated Gupta et al. (2021)'s dataset were located in the tropics and none in our study area, and that the soil datasets used in their methodology are likely to have substantial differences to the one we generated in our study, such as the clay fraction. At the same time, our comparison of SOL_K values were based on the use of the PTF from Saxton and Rawls (2006), which exhibited the lowest SOL_K results from all PTFs used in this study (Table 6), and were developed using data from

North America, which can lead to high errors and uncertainty when used in other regions (Vereecken et al., 2016). Nevertheless, our hybrid framework was able to generate a soil map with high accuracy (mean $r^2 > 0.9$, Table 3) and low mean uncertainty (< 10%, Fig. 6) thus capturing the variability of soil properties that are used to drive most common PTFs.

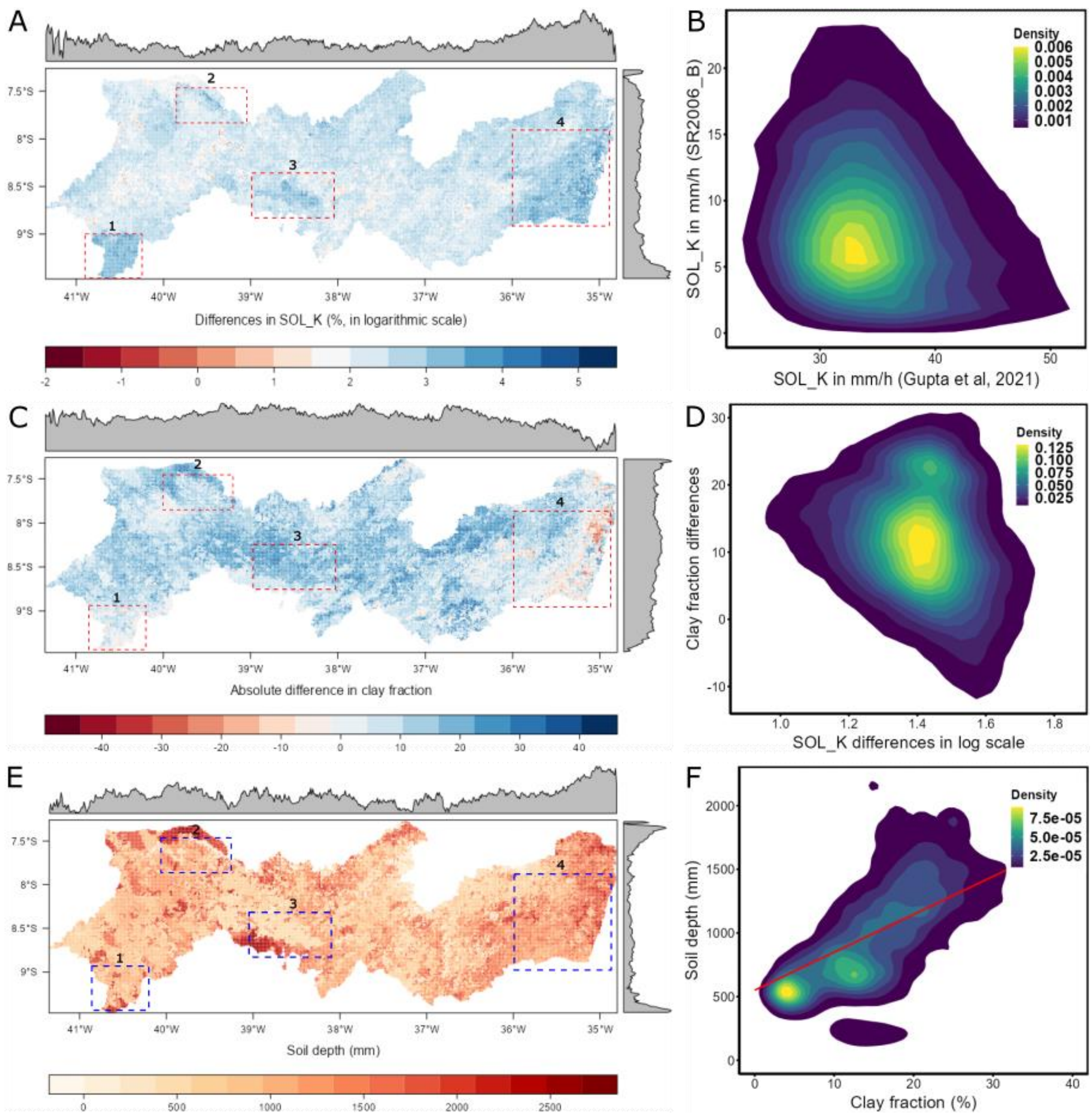

Figure 8. Differences in saturated hydraulic conductivity (SOL_K) and clay fraction between the results from Gupta et al. (2021) and our study, and total soil depth. The maps (panels A, C, and E) highlight areas (within dashed lines) where the SOL_K differences were the greatest, and the top

and right margins exhibit the distribution of the latitudinal and longitudinal means, respectively. The density estimates in panels B, D, and F, were calculated using the kde2d function available in the MASS package (Venables & Ripley, 2003) in the R language (R Core Team, 2017).

3.4 Land cover types and soil texture linkages

Our results show a predominance of high sandy content with a higher density of points exhibiting a 40–70% content for sandy, followed by 20–45% for clay, and 15–25% for silt (Fig. 9). The highest clay content values were found in the East of the Pernambuco State region, covering an area extending from about 20 to 100 km from the coast (Fig. 10). For the remaining area, the sand content is approximately twice higher, and the highest silt content is found within the transition of high clay to sandy areas. There are a few coarse sand-dominated soil patches in sedimentary basins, such as the Jatobá, Belmonte and Fátima, in coastal lowlands, and smaller portions in the coastal plateaus close to the Atlantic Ocean. Moreover, in the West of the study area, there are sandy surface layers at the top of the Araripe plateau.

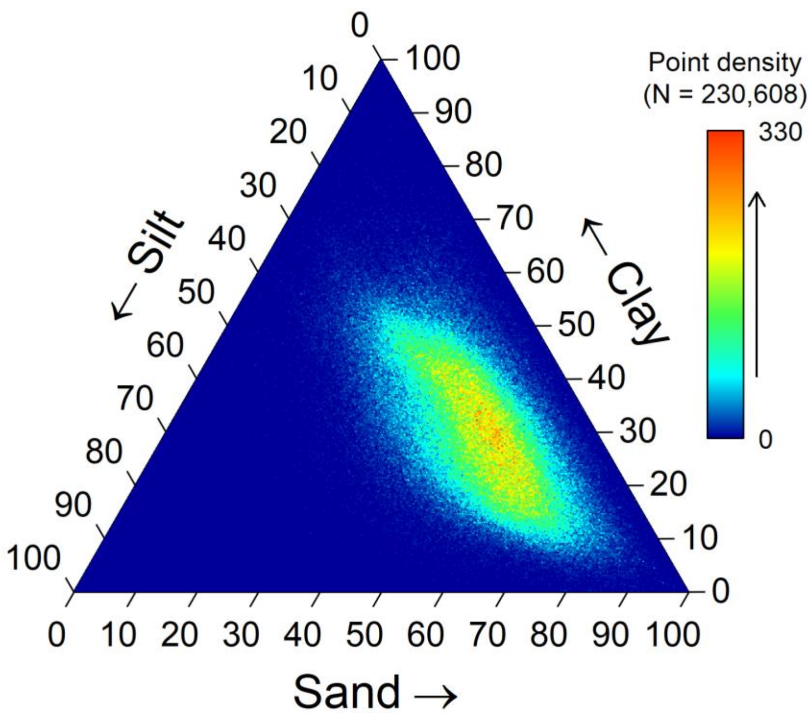

Figure 9. Modeled soil textural distribution for sand, silt and clay.

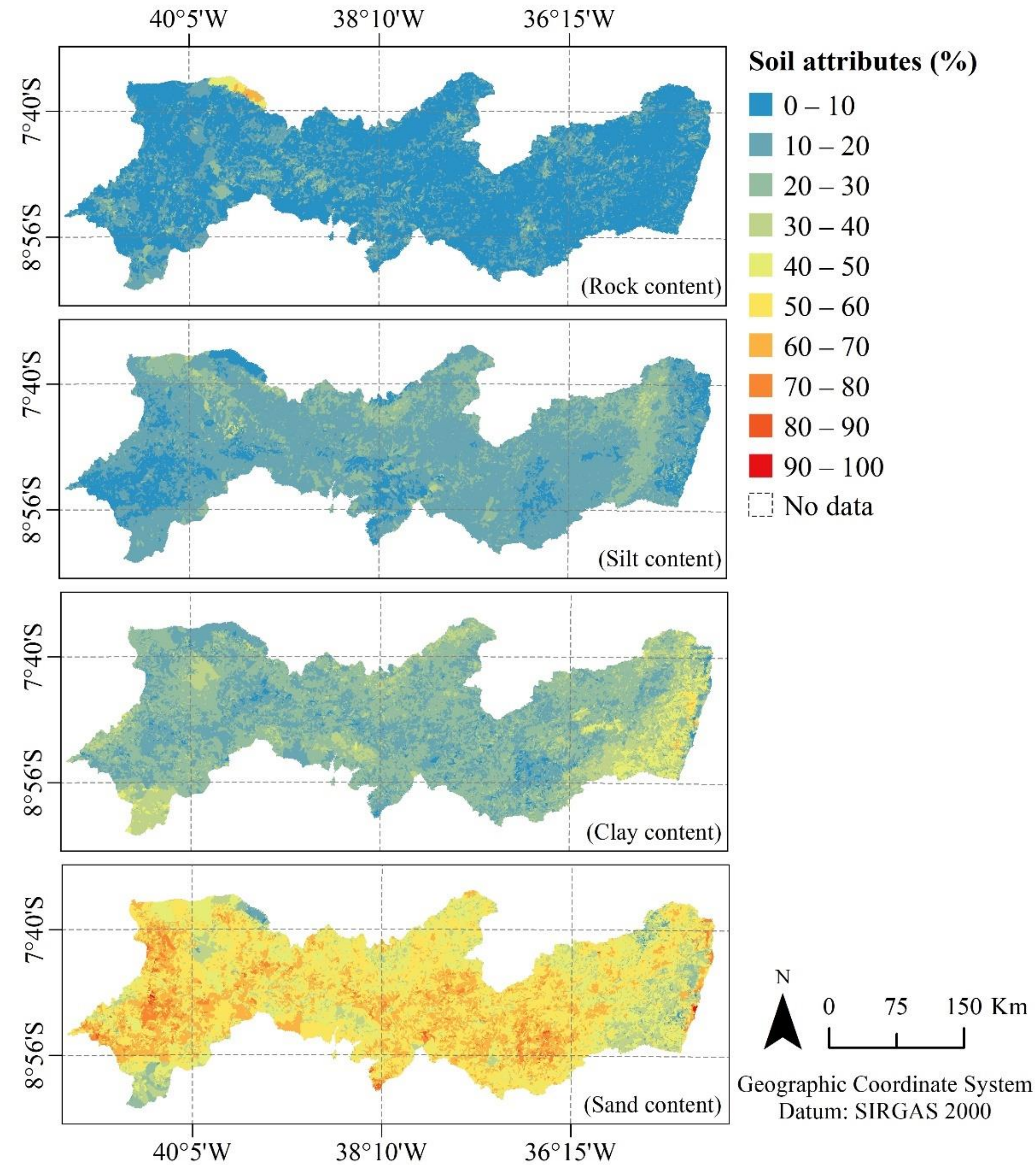

Figure 10. Maps of the modeled soil texture attributes over the study area.

Not surprisingly, the soils with the highest clay content are covered with agricultural fields (Fig. 11) since higher soil water retention is expected as soils particle distribution gets finer (Newman, 1984). Over these patches of higher clay content, agriculture practices vary across the study area due to contrasting precipitation patterns. In the East, the precipitation is the highest and water-intensive sugar cane plantations are predominant over the areas with the highest clay content (38.9% ± 10.6%). In the Southernmost part of our study area, where the climate is dry with low precipitation rates, there is a region with relatively high clay content (over 30%) known as the São Francisco Valley; there, perennial crops are maintained via irrigation systems supplied with water from the San Francisco River, which crosses the valley.

We found that approximately 50% of the entire study area had at least one type of land-cover conversion over the 1985–2019 period. The joint analysis of land-use changes and high-resolution robust soil mapping is only one of the applications that is possible with the use of the methodology we propose. For example, since the expansion of agriculture has been towards areas with higher clay content, our results can support the development of strategic plans to improve the use of poorly managed areas with high clay content. Moreover, our maps can be used as evidence in support of environmental policies to prioritize the protection of native vegetation in clayey soils that are particularly vulnerable to deforestation.

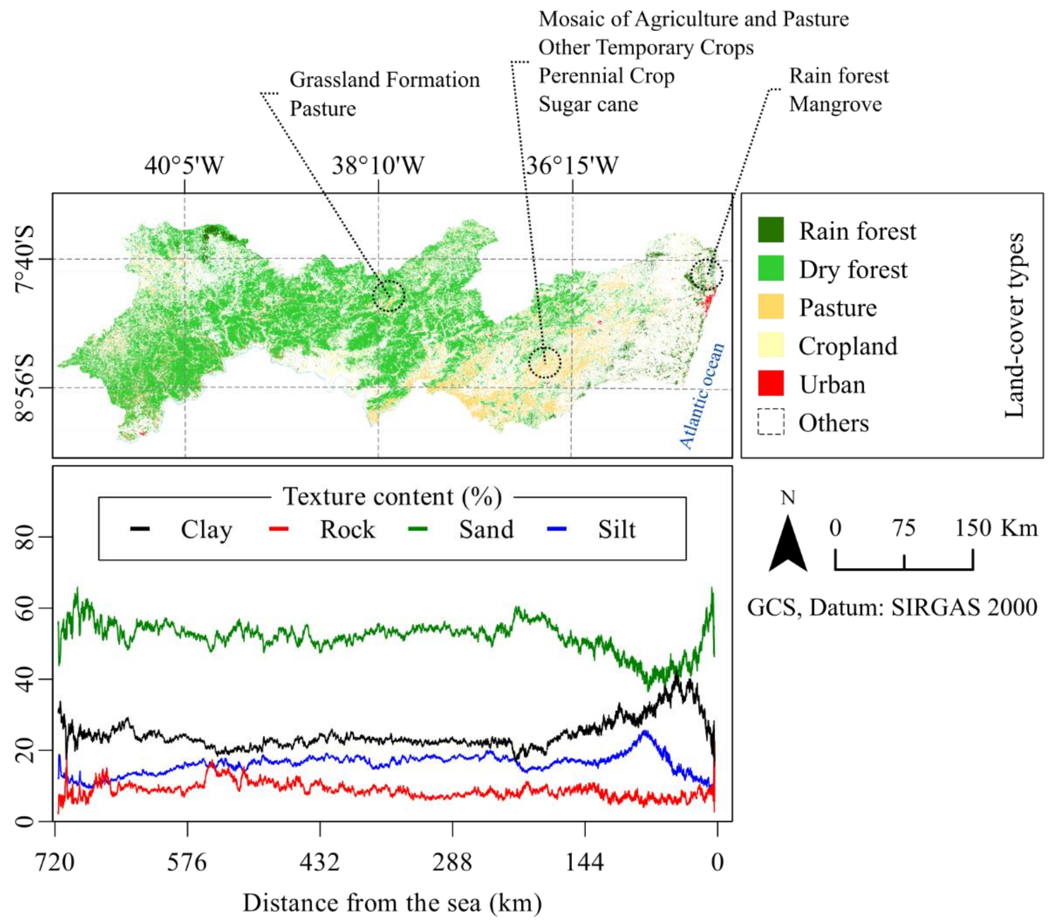

Figure 11. Modeled soil texture attributes and land-cover across the study area.

4 Conclusions

In this study we produced a robust soil map using inductive ML techniques based on decision trees for a region with highly variable topography, climate, and vegetation characteristics that is not well represented in global datasets of soil properties. Good model performance is reflected in our models' statistics that presents r^2 and PBIAS values varying from 0.79 to 0.98, and from -1.39 to 1.14, respectively. The advantage of decision tree methods can be far greater than classical linear regression because decision tree methods are entirely free of strict assumptions, and all types of variables, scales, distributions, and relations can be handled jointly and simultaneously. We explored this characteristic in detail in this study, by employing multiple freely available datasets with an extensive range of data types (e.g., number of soil layers and chemical composition) to improve the soil information in our study area. Although GBM may be considered semi-black-box models, adding a feature selector in the calibration processing allowed us to perform uncertainty analyses and pinpoint the main environmental modulators of different soil properties.

Our results are especially important for soil management in response to climate change or land use and land management changes, such as deforestation and desertification, at multiple spatial scales. The novel hybrid machine learning framework includes enhanced flexibility, the possibility of producing regular short-term map updates, and supporting future economic and environmental modeling integration (e.g., https://super.hawqs.tamu.edu/), while drastically reducing capital investments compared to *in situ* surveys and mapping. We believe that these promising findings will improve all modeling efforts that require detailed soil information, including land surface and hydrological modelling, and will encourage the development of new frameworks and datasets for soil sciences. Our new dataset can be further used to create a new portfolio of applications, such as agricultural zoning and environmental management strategies.

Acknowledgments

We thank Surya Gupta for clarifying aspects on Gupta et al. (2021) that allowed us to use and compare it to our results. Soil data access was provided by the Brazilian Agricultural Research Corporation (EMBRAPA) through the Agroecological Zoning of the state of Pernambuco (ZAPE) project. The authors also acknowledge the following funding sources: The Brazilian Coordination for the Improvement of Higher Level Personnel (CAPES 88887.371850/2019-00) for AGSSS and JDG; The Fundação de Amparo a Ciência e Tecnologia do Estado de Pernambuco (Project FACEPE APQ, 0646-9.25/16) for RQM and JDG; The National Council for Scientific and Technological Development of Brazil (CNPq) through the projects MCTIC/CNPq 28/2018 (431980/2018-7), PEGASUS MCTI/CNPq Nº 19/2017 (441305/2017-2), CNPq/MCTIC/BRICS 29/2017 (442335/2017-2), INCT Mudanças Climáticas II, and productivity grants (448236/2014-1 and 313469/2020-2) for SMGLM and MSBA; and the UK Natural Environment Research Council (NE/N012526/1 ICL and NE/N012488/1 UoR) and FAPESP (The São Paulo Research Foundation) (FAPESP 2015/50488-5) for the UK/Brazil Nordeste project for AV, RLBN and MSBM.

Data Availability Statement

The code developed and used in this study is freely available at the GitHub repository (https://github.com/razeayres/sleepy) (Miranda, Nóbrega, & Galvíncio, 2022). The datasets generated and analyzed in this study are available at the Zenodo repository (https://zenodo.org/record/5918544) (Miranda, Nóbrega, da Silva, et al., 2022). The observed data used to support the findings of this study are in paper format in the archives from the Agroecological Zoning of the state of Pernambuco (ZAPE) project of the Brazilian Agricultural Research Corporation (EMBRAPA), they are not licensed for redistribution, and access to it can be acquired by contacting the EMBRAPA Soil Unit at cnps.sac@embrapa.br.

References

ABNT. (1995). *Rochas e Solo* (No. NBR 6502). Rio de Janeiro: Associação Brasileira de Normas Técnicas.

Adhikari, K., Hartemink, A. E., Minasny, B., Bou Kheir, R., Greve, M. B., & Greve, M. H. (2014). Digital mapping of soil organic carbon contents and stocks in Denmark. *PloS One*, *9*(8), e105519. https://doi.org/10.1371/journal.pone.0105519

Akpa, S. I. C., Odeh, I. O. A., Bishop, T. F. A., Hartemink, A. E., & Amapu, I. Y. (2016). Total soil organic carbon and carbon sequestration potential in Nigeria. *Geoderma*, *271*, 202–215. https://doi.org/10.1016/j.geoderma.2016.02.021

Alvares, C. A., Stape, J. L., Sentelhas, P. C., de Moraes Gonçalves, J. L., & Sparovek, G. (2013). Köppen's climate classification map for Brazil. *Meteorologische Zeitschrift*, *22*(6), 711–728. https://doi.org/10.1127/0941-2948/2013/0507

Araujo Filho, J. C. de, Burgos, N., Lopes, O. F., Silva, F. H. B. B. da, Medeiros, L. A. R., Melo Filho, H. F. R. de, et al. (2000). *Levantamento de reconhecimento de baixa e média intensidade dos solos do Estado de Pernambuco* (Vol. 11). Rio de Janeiro: Embrapa Solos. Retrieved from https://www.infoteca.cnptia.embrapa.br/infoteca/handle/doc/337631

Araújo Filho, J. C. de, Araújo, M. do S. B. de, Marques, F. A., & Lopes, H. L. (2014). Solos. In F. S. de M. Torres & P. A. dos S. Pfaltzgraff (Eds.), *Geodiversidade do estado de Pernambuco*. MINISTÉRIO DE MINAS E ENERGIA.

Arnold, J. G., Srinivasan, R., Muttiah, R. S., & Williams, J. R. (1998). Large area hydrologic modeling and assessment part i: Model development. *Journal of the American Water Resources Association*, *34*(1), 73–89. https://doi.org/10.1111/j.1752-1688.1998.tb05961.x

Arrouays, D., McKenzie, N., Hempel, J., de Forges, A. R., & McBratney, A. B. (2014). *GlobalSoilMap: Basis of the global spatial soil information system*. CRC Press. Retrieved from https://play.google.com/store/books/details?id=S5ClAgAAQBAJ

Badía, D., Ruiz, A., Girona, A., Martí, C., Casanova, J., Ibarra, P., & Zufiaurre, R. (2016). The influence of elevation on soil properties and forest litter in the Siliceous Moncayo Massif, SW Europe. *Journal of Mountain Science*, *13*(12), 2155–2169. https://doi.org/10.1007/s11629-015-3773-6

Ballabio, C., Panagos, P., & Monatanarella, L. (2016). Mapping topsoil physical properties at European scale using the LUCAS database. *Geoderma*, *261*, 110–123. https://doi.org/10.1016/j.geoderma.2015.07.006

Barbieri, D. M., Marques Júnior, J., Alleoni, L. R. F., Garbuio, F. J., & Camargo, L. A. (2009). Hillslope curvature, clay mineralogy, and phosphorus adsorption in an Alfisol cultivated with sugarcane. *Scientia Agricola*, *66*(6), 819–826. https://doi.org/10.1590/s0103-90162009000600015

Barros, A. H. C., & de Jong van Lier, Q. (2014). Pedotransfer functions for Brazilian soils. In *Application of Soil Physics in Environmental Analyses* (pp. 131–162). Cham: Springer International Publishing. https://doi.org/10.1007/978-3-319-06013-2_6

Barros, A. H. C., van Lier, Q. de J., Maia, A. de H. N., & Scarpare, F. V. (2013). Pedotransfer functions to estimate water retention parameters of soils in northeastern Brazil. *Revista Brasileira de Ciencia Do Solo*, *37*(2), 379–391. https://doi.org/10.1590/s0100-06832013000200009

Begueria, S., Spanu, V., Navas, A., Machin, J., & Angulo-Martinez, M. (2013). Modeling the spatial distribution of soil properties by generalized least squares regression: Toward a general theory of spatial variates. *Journal of Soil and Water Conservation*, *68*(3), 172–184. https://doi.org/10.2489/jswc.68.3.172

Behrens, T., Schmidt, K., Viscarra Rossel, R. A., Gries, P., Scholten, T., & MacMillan, R. A. (2018). Spatial modelling with Euclidean distance fields and machine learning. *European Journal of Soil Science*, *69*(5), 757–770. https://doi.org/10.1111/ejss.12687

Belk, E. L., Markewitz, D., Rasmussen, T. C., Carvalho, E. J. M., Nepstad, D. C., & Davidson, E. A. (2007). Modeling the effects of throughfall reduction on soil water content in a Brazilian Oxisol under a moist tropical forest. *Water Resources Research*, *43*(8). https://doi.org/10.1029/2006wr005493

Benites, V. de M., Machado, P. O. de A., Fidalgo, E. C. C., Coelho, M. R., Madari, B. E., & Lima, C. X. (2006). *Funções de pedotransferência para estimativa da densidade dos solos brasileiros* (No. 104). Rio de Janeiro: Embrapa Solos, 2006. Retrieved from https://www.infoteca.cnptia.embrapa.br/handle/doc/881919?locale=es

Benites, V. M., Machado, P. L. O. A., Fidalgo, E. C. C., Coelho, M. R., & Madari, B. E. (2007). Pedotransfer functions for estimating soil bulk density from existing soil survey reports in Brazil. *Geoderma*, *139*(1–2), 90–97. https://doi.org/10.1016/j.geoderma.2007.01.005

Best, M. J., Pryor, M., Clark, D. B., Rooney, G. G., Essery, R. L. H., Ménard, C. B., et al. (2011). The Joint UK Land Environment Simulator (JULES), model description – Part 1: Energy and water fluxes. *Geoscientific Model Development*, *4*(3), 677–699. https://doi.org/10.5194/gmd-4-677-2011

Bonan, G. B. (2008). Forests and Climate Change : Forcings, Feebacks, and the Climate Benefits of Forests. *Science*, *320*(June), 1444–1450. https://doi.org/10.1126/science.1155121

Boschi, R. S., Bocca, F. F., Lopes-Assad, M. L. R. C., & Assad, E. D. (2018). How accurate are pedotransfer functions for bulk density for Brazilian soils? *Scientia Agricola*, *75*(1), 70–78. https://doi.org/10.1590/1678-992x-2016-0357

Bossa, A. Y., Diekkrüger, B., Igué, A. M., & Gaiser, T. (2012). Analyzing the effects of different soil databases on modeling of hydrological processes and sediment yield in Benin (West Africa). *Geoderma*, *173–174*, 61–74. https://doi.org/10.1016/j.geoderma.2012.01.012

Bouma, J., & McBratney, A. (2013). Framing soils as an actor when dealing with wicked environmental problems. *Geoderma*, *200–201*, 130–139. https://doi.org/10.1016/j.geoderma.2013.02.011

Brunke, M. A., Broxton, P., Pelletier, J., Gochis, D., Hazenberg, P., Lawrence, D. M., et al. (2016). Implementing and evaluating variable soil thickness in the Community Land Model, version 4.5 (CLM4.5). *Journal of Climate*, *29*(9), 3441–3461. https://doi.org/10.1175/jcli-d-15-0307.1

Chawla, N. V., Bowyer, K. W., Hall, L. O., & Kegelmeyer, W. P. (2002). SMOTE: Synthetic minority over-sampling technique. *The Journal of Artificial Intelligence Research*, *16*, 321–357. https://doi.org/10.1613/jair.953

Clark, D. B., Mercado, L. M., Sitch, S., Jones, C. D., Gedney, N., Best, M. J., et al. (2011). The Joint UK Land Environment Simulator (JULES), model description – Part 2: Carbon fluxes and vegetation dynamics. *Geoscientific Model Development*, *4*(3), 701–722. https://doi.org/10.5194/gmd-4-701-2011

Dai, Y., Xin, Q., Wei, N., Zhang, Y., Shangguan, W., Yuan, H., et al. (2019). A global high-resolution data set of soil hydraulic and thermal properties for land surface modeling. *Journal of Advances in Modeling Earth Systems*, *11*(9), 2996–3023. https://doi.org/10.1029/2019ms001784

Dai, Y., Shangguan, W., Wei, N., Xin, Q., Yuan, H., Zhang, S., et al. (2019). A review of the global soil property maps for Earth system models. *SOIL*, *5*(2), 137–158. https://doi.org/10.5194/soil-5-137-2019

Davarzani, H., Smits, K., Tolene, R. M., & Illangasekare, T. (2014). Study of the effect of wind speed on evaporation from soil through integrated modeling of the atmospheric boundary layer and shallow subsurface. *Water Resources Research, 50*(1), 661–680. https://doi.org/10.1002/2013WR013952

De Vos, B., Van Meirvenne, M., Quataert, P., Deckers, J., & Muys, B. (2005). Predictive quality of pedotransfer functions for estimating bulk density of forest soils. *Soil Science Society of America Journal. Soil Science Society of America*, *69*(2), 500–510. https://doi.org/10.2136/sssaj2005.0500

Didan, K. (2015). MOD13A3 MODIS/Terra Vegetation Indices Monthly L3 Global 1km SIN Grid V006 [Data set]. NASA EOSDIS Land Processes DAAC. https://doi.org/10.5067/MODIS/MOD13A3.006

Dixon, J. L., Chadwick, O. A., & Vitousek, P. M. (2016). Climate-driven thresholds for chemical weathering in postglacial soils of New Zealand. *Journal of Geophysical Research. Earth Surface*, *121*(9), 1619–1634. https://doi.org/10.1002/2016jf003864

Dy, C. Y., & Fung, J. C. H. (2016). Updated global soil map for the Weather Research and Forecasting model and soil moisture initialization for the Noah land surface model. *Journal of Geophysical Research Atmospheres*, *121*(15), 8777–8800. https://doi.org/10.1002/2015jd024558

Elith, J., Leathwick, J. R., & Hastie, T. (2008). A working guide to boosted regression trees. *The Journal of Animal Ecology*, *77*(4), 802–813. https://doi.org/10.1111/j.1365-2656.2008.01390.x

Ellili-Bargaoui, Y., Malone, B. P., Michot, D., Minasny, B., Vincent, S., Walter, C., & Lemercier, B. (2020). Comparing three approaches of spatial disaggregation of legacy soil maps based on the Disaggregation and Harmonisation of Soil Map Units Through Resampled Classification Trees (DSMART) algorithm. *SOIL*, *6*(2), 371–388. https://doi.org/10.5194/soil-6-371-2020

Embrapa. (1997). *Manual de Métodos de Análise de Solo* (2nd ed., p. 212). Rio de Janeiro: EMBRAPA-CNPS.

Eppes, M. C., Magi, B., Scheff, J., Warren, K., Ching, S., & Feng, T. (2020). Warmer, wetter climates accelerate mechanical weathering in field data, independent of stress-loading. *Geophysical Research Letters*, *47*(24). https://doi.org/10.1029/2020gl089062

Esfandiarpour-Boroujeni, I., Shahini-Shamsabadi, M., Shirani, H., Mosleh, Z., Bagheri-Bodaghabadi, M., & Salehi, M. H. (2020). Assessment of different digital soil mapping methods for prediction of soil classes in the Shahrekord plain, Central Iran. *Catena*, *193*(104648), 104648. https://doi.org/10.1016/j.catena.2020.104648

F. Dormann, C., M. McPherson, J., B. Araújo, M., Bivand, R., Bolliger, J., Carl, G., et al. (2007). Methods to account for spatial autocorrelation in the analysis of species distributional data: a review. *Ecography*, *30*(5), 609–628. https://doi.org/10.1111/j.2007.0906-7590.05171.x

Fatichi, S., Or, D., Walko, R., Vereecken, H., Young, M. H., Ghezzehei, T. A., et al. (2020). Soil structure is an important omission in Earth System Models. *Nature Communications*, *11*(1), 522. https://doi.org/10.1038/s41467-020-14411-z

van Genuchten, M. T. (1980). A Closed-form Equation for Predicting the Hydraulic Conductivity of Unsaturated Soils. *Soil Science Society of America Journal*, *44*(5), 892–898. https://doi.org/10.2136/sssaj1980.03615995004400050002x

Gessler, P. E., Moore, I. D., McKENZIE, N. J., & Ryan, P. J. (1995). Soil-landscape modelling and spatial prediction of soil attributes. *International Journal of Geographical Information Systems*, *9*(4), 421–432. https://doi.org/10.1080/02693799508902047

Gray, J. M., Bishop, T. F. A., & Smith, P. L. (2016). Digital mapping of pre-European soil carbon stocks and decline since clearing over New South Wales, Australia. *Soil Research*, *54*(1), 49. https://doi.org/10.1071/sr14307

Greenbelt. (2019). Earthdata Search. Earth Science Data and Information System (ESDIS) Project, Earth Science Projects Division (ESPD), Flight Projects Directorate, Goddard Space Flight Center (GSFC) National Aeronautics and Space Administration (NASA). Retrieved April 11, 2021, from https://search.earthdata.nasa.gov/

Guevara, M., Olmedo, G. F., Stell, E., Yigini, Y., Aguilar Duarte, Y., Arellano Hernández, C., et al. (2018). No silver bullet for digital soil mapping: country-specific soil organic carbon estimates across Latin America. *SOIL*, *4*(3), 173–193. https://doi.org/10.5194/soil-4-173-2018

Gupta, S., Lehmann, P., Bonetti, S., Papritz, A., & Or, D. (2021). Global prediction of soil saturated hydraulic conductivity using random forest in a covariate-based GeoTransfer function (CoGTF) framework. *Journal of Advances in Modeling Earth Systems*, *13*(4). https://doi.org/10.1029/2020ms002242

Guyon, I., Weston, J., Barnhill, S., & Vapnik, V. (2002). *Machine Learning*, *46*(1/3), 389–422. https://doi.org/10.1023/a:1012487302797

Hartemink, A. E., Lowery, B., & Wacker, C. (2012). Soil maps of Wisconsin. *Geoderma*, *189–190*, 451–461. https://doi.org/10.1016/j.geoderma.2012.05.025

Hawkins, D. M. (2004). The problem of overfitting. *Journal of Chemical Information and Computer Sciences*, *44*(1), 1–12. https://doi.org/10.1021/ci0342472

Hengl, T. (2018). Clay content in % (kg / kg) at 6 standard depths (0, 10, 30, 60, 100 and 200 cm) at 250 m resolution [Data set]. Zenodo. https://doi.org/10.5281/ZENODO.2525663

Hengl, T., Mendes de Jesus, J., Heuvelink, G. B. M., Ruiperez Gonzalez, M., Kilibarda, M., Blagotić, A., et al. (2017). SoilGrids250m: Global gridded soil information based on machine learning. *PloS One*, *12*(2), e0169748. https://doi.org/10.1371/journal.pone.0169748

Hitziger, M., & Ließ, M. (2014). Comparison of three supervised learning methods for digital soil mapping: Application to a complex terrain in the Ecuadorian Andes. *Applied and Environmental Soil Science*, *2014*, 1–12. https://doi.org/10.1155/2014/809495

Kearney, M. R., & Maino, J. L. (2018). Can next-generation soil data products improve soil moisture modelling at the continental scale? An assessment using a new microclimate package for the R programming environment. *Journal of Hydrology*, *561*, 662–673. https://doi.org/10.1016/j.jhydrol.2018.04.040

Kempen, B., Brus, D. J., Stoorvogel, J. J., Heuvelink, G. B. M., & de Vries, F. (2012). Efficiency comparison of conventional and digital soil mapping for updating soil maps. *Soil Science Society of America Journal. Soil Science Society of America*, *76*(6), 2097–2115. https://doi.org/10.2136/sssaj2011.0424

Krinner, G., Viovy, N., de Noblet-Ducoudré, N., Ogée, J., Polcher, J., Friedlingstein, P., et al. (2005). A dynamic global vegetation model for studies of the coupled atmosphere-biosphere system. *Global Biogeochemical Cycles*, *19*(1). https://doi.org/10.1029/2003gb002199

Krysanova, V., Hattermann, F., & Wechsung, F. (2005). Development of the ecohydrological model SWIM for regional impact studies and vulnerability assessment. *Hydrological Processes*, *19*(3), 763–783. https://doi.org/10.1002/hyp.5619

Lagacherie, P., & McBratney, A. B. (2006). Chapter 1 spatial soil information systems and spatial soil inference systems: Perspectives for digital soil mapping. In *Developments in Soil Science* (pp. 3–22). Elsevier. https://doi.org/10.1016/s0166-2481(06)31001-x

Laurent, F., Poccard-Chapuis, R., Plassin, S., & Pimentel Martinez, G. (2017). Soil texture derived from topography in North-eastern Amazonia. *Journal of Maps*, *13*(2), 109–115. https://doi.org/10.1080/17445647.2016.1266524

Li, J., & Heap, A. D. (2014). Spatial interpolation methods applied in the environmental sciences: A review. *Environmental Modelling & Software: With Environment Data News*, *53*, 173–189. https://doi.org/10.1016/j.envsoft.2013.12.008

McBratney, A. B., Mendonça Santos, M. L., & Minasny, B. (2003). On digital soil mapping. *Geoderma*, *117*(1–2), 3–52. https://doi.org/10.1016/s0016-7061(03)00223-4

Mendonça-Santos, M. L., & dos Santos, H. G. (2006). Chapter 3 the state of the art of Brazilian soil mapping and prospects for digital soil mapping. In *Developments in Soil Science* (pp. 39–601). Elsevier. https://doi.org/10.1016/s0166-2481(06)31003-3

Minasny, B., & Hartemink, A. E. (2011). Predicting soil properties in the tropics. *Earth-Science Reviews*, *106*(1–2), 52–62. https://doi.org/10.1016/j.earscirev.2011.01.005

Miranda, R. de Q., Nóbrega, R. L. B., da Silva, E. L. R., da Silva, J. F., de Araújo Filho, J. C., de Moura, M. S. B., et al. (2022). Model outputs from the study “Hybrid machine learning for digital soil mapping across a longitudinal gradient of contrasting topography, climate and vegetation” [Data set]. Zenodo. https://doi.org/10.5281/ZENODO.5918544

Miranda, R. de Q., Nóbrega, R. L. B., & Galvíncio, J. D. (2022). SLEEPy - an implementation of the Soil-Landscape Estimation and Evaluation Program using machine learning modeling (Version 1.1) [Python]. Github. Retrieved from https://github.com/razeayres/sleepy

Montzka, C., Herbst, M., Weihermüller, L., Verhoef, A., & Vereecken, H. (2017). A global data set of soil hydraulic properties and sub-grid variability of soil water retention and hydraulic conductivity curves. *Earth System Science Data*, *9*(2), 529–543. https://doi.org/10.5194/essd-9-529-2017

Moore, I. D., Gessler, P. E., Nielsen, G. A., & Peterson, G. A. (1993). Soil attribute prediction using terrain analysis. *Soil Science Society of America Journal. Soil Science Society of America*, *57*(2), 443–452. https://doi.org/10.2136/sssaj1993.03615995005700020026x

de Morisson Valeriano, M., & de Fátima Rossetti, D. (2012). Topodata: Brazilian full coverage refinement of SRTM data. *Applied Geography (Sevenoaks, England)*, *32*(2), 300–309. https://doi.org/10.1016/j.apgeog.2011.05.004

Natekin, A., & Knoll, A. (2013). Gradient boosting machines, a tutorial. *Frontiers in Neurorobotics*, *7*. https://doi.org/10.3389/fnbot.2013.00021

Nettesheim, F. C., Conto, T. de, Pereira, M. G., & Machado, D. L. (2015). Contribution of topography and incident solar radiation to variation of soil and plant litter at an area with heterogeneous terrain. *Revista Brasileira de Ciencia Do Solo*, *39*(3), 750–762. https://doi.org/10.1590/01000683rbcs20140459

Newman, A. C. D. (1984). The significance of clays in agriculture and soils. *Philosophical Transactions of the Royal Society of London*, *311*(1517), 375–389. https://doi.org/10.1098/rsta.1984.0035

Nketia, K. A., Asabere, S. B., Ramcharan, A., Herbold, S., Erasmi, S., & Sauer, D. (2022). Spatio-temporal mapping of soil water storage in a semi-arid landscape of northern Ghana – A multi-tasked ensemble machine-learning approach. *Geoderma*, *410*(115691), 115691. https://doi.org/10.1016/j.geoderma.2021.115691

Oliveira, D. P., Sartor, L. R., Souza Júnior, V. S., Corrêa, M. M., Romero, R. E., Andrade, G. R. P., & Ferreira, T. O. (2018). Weathering and clay formation in semi-arid calcareous soils from Northeastern Brazil. *Catena*, *162*, 325–332. https://doi.org/10.1016/j.catena.2017.10.030

Oliveira, L. B., Ribeiro, M. R., Jacomine, P. K. T., Rodrigues, J. J. V., & Marques, F. A. (2002). Funções de pedotransferência para predição da umidade retida a potenciais específicos em solos do estado de Pernambuco. *Revista Brasileira de Ciencia Do Solo*, *26*(2), 315–323. https://doi.org/10.1590/s0100-06832002000200004

Orgiazzi, A., Bardgett, R. D., Barrios, E., Behan-Pelletier, V., Briones, M. J. I., Chotte, J.-L., et al. (Eds.). (2016). *Global soil biodiversity atlas*. Luxembourg: European Commission, Publications Office of the European Union. Retrieved from https://data.europa.eu/doi/10.2788/2613

Ottoni, M. V., Ottoni Filho, T. B., Schaap, M. G., Lopes-Assad, M. L. R. C., & Rotunno Filho, O. C. (2018). Hydrophysical database for Brazilian soils (HYBRAS) and pedotransfer functions for water retention. *Vadose Zone Journal: VZJ*, *17*(1), 1–17. https://doi.org/10.2136/vzj2017.05.0095

Overmars, K. P., de Groot, W. T., & Huigen, M. G. A. (2007). Comparing inductive and deductive modeling of land use decisions: Principles, a model and an illustration from the Philippines.

Human Ecology: An Interdisciplinary Journal, *35*(4), 439–452. https://doi.org/10.1007/s10745-006-9101-6

Padarian, J., Minasny, B., & McBratney, A. B. (2017). Chile and the Chilean soil grid: A contribution to GlobalSoilMap. *Geoderma Regional*, *9*, 17–28. https://doi.org/10.1016/j.geodrs.2016.12.001

Pahlavan-Rad, M. R., Dahmardeh, K., Hadizadeh, M., Keykha, G., Mohammadnia, N., Gangali, M., et al. (2020). Prediction of soil water infiltration using multiple linear regression and random forest in a dry flood plain, eastern Iran. *Catena*, *194*(104715), 104715. https://doi.org/10.1016/j.catena.2020.104715

Paschalis, A., Bonetti, S., Guo, Y., & Fatichi, S. (2022). On the uncertainty induced by pedotransfer functions in terrestrial biosphere modeling. *Water Resources Research*, *58*(9). https://doi.org/10.1029/2021wr031871

Patton, N. R., Lohse, K. A., Godsey, S. E., Crosby, B. T., & Seyfried, M. S. (2018). Predicting soil thickness on soil mantled hillslopes. *Nature Communications*, *9*(1), 3329. https://doi.org/10.1038/s41467-018-05743-y

Poggio, L., & Gimona, A. (2017). Assimilation of optical and radar remote sensing data in 3D mapping of soil properties over large areas. *The Science of the Total Environment*, *579*, 1094–1110. https://doi.org/10.1016/j.scitotenv.2016.11.078

Poppiel, R. R., Demattê, J. A. M., Rosin, N. A., Campos, L. R., Tayebi, M., Bonfatti, B. R., et al. (2021). High resolution middle eastern soil attributes mapping via open data and cloud computing. *Geoderma*, *385*(114890), 114890. https://doi.org/10.1016/j.geoderma.2020.114890

Pribyl, D. W. (2010). A critical review of the conventional SOC to SOM conversion factor. *Geoderma*, *156*(3–4), 75–83. https://doi.org/10.1016/j.geoderma.2010.02.003

R Core Team. (2017). R: A language and environment for statistical computing (Version 3.3.3). Vienna, Austria: R Foundation for Statistical Computing. Retrieved from https://www.r-project.org/

Rahmati, M., Weihermüller, L., Vanderborght, J., Pachepsky, Y. A., Mao, L., Sadeghi, S. H., et al. (2018). Development and analysis of the Soil Water Infiltration Global database. *Earth System Science Data*, *10*(3), 1237–1263. https://doi.org/10.5194/essd-10-1237-2018

Ramifehiarivo, N., Brossard, M., Grinand, C., Andriamananjara, A., Razafimbelo, T., Rasolohery, A., et al. (2017). Mapping soil organic carbon on a national scale: Towards an improved and updated map of Madagascar. *Geoderma Regional*, *9*, 29–38. https://doi.org/10.1016/j.geodrs.2016.12.002

Ravi, S., D'Odorico, P., Over, T. M., & Zobeck, T. M. (2004). On the effect of air humidity on soil susceptibility to wind erosion: The case of air-dry soils. *Geophysical Research Letters*, *31*(9). https://doi.org/10.1029/2004gl019485

Richards, J. A. (2013). *Remote sensing digital image analysis*. Berlin, Heidelberg: Springer Berlin Heidelberg. https://doi.org/10.1007/978-3-642-30062-2

Salgueiro, J. H. P. de B., Montenegro, S. M. G. L., Pinto, E. J. de A., Silva, B. B. da, Souza, W. M. de, & Oliveira, L. M. M. de. (2016). Influence of oceanic-atmospheric interactions on extreme events of daily rainfall in the Sub-basin 39 located in Northeastern Brazil. *RBRH*, *21*(4), 685–693. https://doi.org/10.1590/2318-0331.011616023

Saxton, K. E., & Rawls, W. J. (2006). Soil water characteristic estimates by texture and organic matter for hydrologic solutions. *Soil Science Society of America Journal. Soil Science Society of America*, *70*(5), 1569. https://doi.org/10.2136/sssaj2005.0117

Scharlemann, J. P. W., Tanner, E. V. J., Hiederer, R., & Kapos, V. (2014). Global soil carbon: understanding and managing the largest terrestrial carbon pool. *Carbon Management*, *5*(1), 81–91. https://doi.org/10.4155/cmt.13.77

Scull, P., Franklin, J., Chadwick, O. A., & McArthur, D. (2003). Predictive soil mapping: a review. *Progress in Physical Geography*, *27*(2), 171–197. https://doi.org/10.1191/0309133303pp366ra

Sharpley, A. N., Williams, J. R., United States, & Agricultural Research Service. (1993). EPIC, Erosion/Productivity Impact Calculator, 1, Model documentation. Retrieved from https://handle.nal.usda.gov/10113/CAT10698097

Souza, C. M., Jr, Z. Shimbo, J., Rosa, M. R., Parente, L. L., A. Alencar, A., Rudorff, B. F. T., et al. (2020). Reconstructing three decades of land use and land cover changes in Brazilian biomes with Landsat archive and earth engine. *Remote Sensing*, *12*(17), 2735. https://doi.org/10.3390/rs12172735

Souza, R., Feng, X., Antonino, A., Montenegro, S., Souza, E., & Porporato, A. (2016). Vegetation response to rainfall seasonality and interannual variability in tropical dry forests. *Hydrological Processes*, *30*(20), 3583–3595. https://doi.org/10.1002/hyp.10953

T. M. Zobeck, D. W. Fryrear, & R. D. Pettit. (1989). Management effects on wind-eroded sediment and plant nutrients. *Journal of Soil and Water Conservation*, *44*(2), 160. Retrieved from http://www.jswconline.org/content/44/2/160.abstract

Taghizadeh-Mehrjardi, R., Nabiollahi, K., & Kerry, R. (2016). Digital mapping of soil organic carbon at multiple depths using different data mining techniques in Baneh region, Iran. *Geoderma*, *266*, 98–110. https://doi.org/10.1016/j.geoderma.2015.12.003

Tan, S., Wang, H., Prentice, I. C., & Yang, K. (2021). Land-surface evapotranspiration derived from a first-principles primary production model. *Environmental Research Letters: ERL [Web Site]*. https://doi.org/10.1088/1748-9326/ac29eb

Tarboton, D. G., Bras, R. L., & Rodriguez-Iturbe, I. (1991). On the extraction of channel networks from digital elevation data. *Hydrological Processes*, *5*(1), 81–100. https://doi.org/10.1002/hyp.3360050107

Teng, H., Viscarra Rossel, R. A., Shi, Z., & Behrens, T. (2018). Updating a national soil classification with spectroscopic predictions and digital soil mapping. *Catena*, *164*, 125–134. https://doi.org/10.1016/j.catena.2018.01.015

Tomasella, J., & Hodnett, M. G. (1998). Estimating soil water retention characteristics from limited data in Brazilian Amazonia. *Soil Science*, *163*(3), 190–202. https://doi.org/10.1097/00010694-199803000-00003

Tomasella, J., Hodnett, M. G., & Rossato, L. (2000). Pedotransfer functions for the estimation of soil water retention in Brazilian soils. *Soil Science Society of America Journal. Soil Science Society of America*, *64*(1), 327–338. https://doi.org/10.2136/sssaj2000.641327x

Torres, F. S. de M., & Pfaltzgraff, P. A. dos S. (Eds.). (2014). *Geodiversidade do estado de Pernambuco*. CPRM. Retrieved from http://rigeo.cprm.gov.br/handle/doc/16771

Tóth, B., Weynants, M., Pásztor, L., & Hengl, T. (2017). 3D soil hydraulic database of Europe at 250 m resolution. *Hydrological Processes*, *31*(14), 2662–2666. https://doi.org/10.1002/hyp.11203

Truu, M., Ostonen, I., Preem, J.-K., Lõhmus, K., Nõlvak, H., Ligi, T., et al. (2017). Elevated air humidity changes soil bacterial community structure in the silver birch stand. *Frontiers in Microbiology*, *8*, 557. https://doi.org/10.3389/fmicb.2017.00557

Turek, M. E., Poggio, L., Batjes, N. H., Armindo, R. A., de Jong van Lier, Q., de Sousa, L., & Heuvelink, G. B. M. (2022). Global mapping of volumetric water retention at 100, 330 and 15 000 cm suction using the WoSIS database. *International Soil and Water Conservation Research*. https://doi.org/10.1016/j.iswcr.2022.08.001

Tziachris, P., Aschonitis, V., Chatzistathis, T., & Papadopoulou, M. (2019). Assessment of spatial hybrid methods for predicting soil organic matter using DEM derivatives and soil parameters. *Catena*, *174*, 206–216. https://doi.org/10.1016/j.catena.2018.11.010

Valentin, C., & Bresson, L.-M. (1992). Morphology, genesis and classification of surface crusts in loamy and sandy soils. *Geoderma*, *55*(3–4), 225–245. https://doi.org/10.1016/0016-7061(92)90085-l

Venables, W. N., & Ripley, B. D. (2003). *Modern Applied Statistics with S*. Springer Science & Business Media. Retrieved from https://play.google.com/store/books/details?id=974c4vKurNkC

Vereecken, H., Schnepf, A., Hopmans, J. W., Javaux, M., Or, D., Roose, T., et al. (2016). Modeling Soil Processes: Review, Key challenges and New Perspectives. *Vadose Zone Journal*. https://doi.org/10.2136/vzj2015.09.0131

Wadoux, A. M. J.-C., Minasny, B., & McBratney, A. B. (2020). Machine learning for digital soil mapping: Applications, challenges and suggested solutions. *Earth-Science Reviews*, *210*, 103359. https://doi.org/10.1016/j.earscirev.2020.103359

Wan, Z., Hook, S., & Hulley, G. (2015). MOD11A2 MODIS/Terra Land Surface Temperature/Emissivity 8-Day L3 Global 1km SIN Grid V006 [Data set]. NASA EOSDIS Land Processes DAAC. https://doi.org/10.5067/MODIS/MOD11A2.006

Wang, Q., Wu, B., Stein, A., Zhu, L., & Zeng, Y. (2018). Soil depth spatial prediction by fuzzy soil-landscape model. *Journal of Soils and Sediments*, *18*(3), 1041–1051. https://doi.org/10.1007/s11368-017-1779-0

Wang, Y. P., Kowalczyk, E., Leuning, R., Abramowitz, G., Raupach, M. R., Pak, B., et al. (2011). Diagnosing errors in a land surface model (CABLE) in the time and frequency domains. *Journal of Geophysical Research*, *116*(G1). https://doi.org/10.1029/2010jg001385

Whitney, A. W. (1971). A direct method of nonparametric measurement selection. *IEEE Transactions on Computers. Institute of Electrical and Electronics Engineers*, *C–20*(9), 1100–1103. https://doi.org/10.1109/t-c.1971.223410

Yost, J. L., & Hartemink, A. E. (2020). How deep is the soil studied – an analysis of four soil science journals. *Plant and Soil*, *452*(1), 5–18. https://doi.org/10.1007/s11104-020-04550-z

Zeraatpisheh, M., Ayoubi, S., Jafari, A., Tajik, S., & Finke, P. (2019). Digital mapping of soil properties using multiple machine learning in a semi-arid region, central Iran. *Geoderma*, *338*, 445–452. https://doi.org/10.1016/j.geoderma.2018.09.006

Zhang, Y., & Schaap, M. G. (2019). Estimation of saturated hydraulic conductivity with pedotransfer functions: A review. *Journal of Hydrology*, *575*, 1011–1030. https://doi.org/10.1016/j.jhydrol.2019.05.058

Ziadat, F. M., Yeganantham, D., Shoemate, D., Srinivasan, R., Narasimhan, B., & Tech, J. (2015). Soil-Landscape Estimation and Evaluation Program (SLEEP) to predict spatial distribution of soil attributes for environmental modeling. *International Journal of Agricultural and Biological Engineering*, *8*(3), 158–172. https://doi.org/10.25165/ijabe.v8i3.1270